

Highlights

Comparison of empirical and particle force-based density segregation models

Soniya Kumawat, Vishnu Kumar Sahu, Anurag Tripathi

- Measurement duration and initial configuration influence empirical parameter values
- Linear model parameters are more sensitive compared to quadratic model parameters
- Empirical models show larger deviations compared to particle force based models

Comparison of empirical and particle force-based density segregation models

Soniya Kumawat^a, Vishnu Kumar Sahu^b, Anurag Tripathi^{a,*}

^aDepartment of Chemical Engineering, Indian Institute of Technology Kanpur, Uttar Pradesh, 208016, India

^bDepartment of Chemical Engineering and Materials Science, University of Minnesota, Minneapolis, MN 55455, USA

Abstract

The empirical and particle force-based models of granular segregation due to density differences among the species are compared in this work. Dependency of the empirical segregation parameters on the initial configuration, the observation time duration, inclination angle, and mixture composition are discussed in detail. The parameters obtained from empirical models are used to predict the steady-state concentration profiles for different density ratios and compositions. In addition, we utilize the predictions from the particle force-based segregation model and compare them with the predictions of the empirical segregation models. Our results show that the linear empirical segregation model predictions agree well with the simulation results for mixtures rich in light species where as quadratic empirical segregation model works better for mixtures rich in heavy species. Particle force-based segregation model, on the other hand, seems to be in very good agreement with the DEM simulation data across all mixture compositions.

Keywords: Granular mixtures, Discrete Element Method, Density segregation, Empirical segregation model, Particle-force based segregation model

1. Introduction

Granular mixtures often undergo segregation during their flow due to differences in the sizes and/or densities of the particles. Variety of geometries such as chute (Tripathi and Khakhar, 2013; Deng et al., 2018; Tripathi et al., 2021), vibrated bed (Yang, 2006; Tai et al., 2010; Jain et al., 2013), hopper (Xiao et al., 2019), heap (Baxter et al., 1998; Schlick et al., 2016; Fan et al., 2017; Deng et al., 2020), and rotating tumbler (Pereira et al., 2014; Schlick et al., 2015b; Chen et al., 2016; Deng et al., 2019) have been used to understand and predict the segregation of granular mixtures. Discrete element method simulations are commonly utilized to obtain various properties of the flowing mixture which are then used to propose segregation models, often in the form of correlations. These segregation models are typically used in the continuum framework by employing the convection-diffusion equation to predict the concentration of different species in flowing granular mixtures.

One of the most popular approaches for proposing these segregation models involves empirically correlating the species segregation velocity to the flow properties of the mixture. Early researchers investigating segregation of different size mixtures (Savage and Lun (1988); Gray and Chugunov (2006); Gray and Ancy (2011)) assumed the segregation velocity of the species to be linearly dependent on the concentration of other species. Using the segregation model of Gray and Chugunov (2006), however, showed significant difference from the experimental concentration profiles for a binary mixture of different size grains

in the study of Wiederseiner et al. (2011). The authors attributed these differences in the concentration profiles to possible dependence of the segregation velocity on the local shear rate. Later studies (Fan et al. (2014); Schlick et al. (2015a)) confirmed this local shear rate dependency of the segregation velocity and utilized the combined shear rate and concentration dependent segregation velocity to predict size segregation in heap flow. Both linear (Fan et al. (2014); Schlick et al. (2015a, 2016); Deng et al. (2018, 2019, 2020); Gao et al. (2021)) as well as nonlinear (Gajjar and Gray (2014); Van der Vaart et al. (2015); Jones et al. (2018)) forms have been proposed to account for the concentration dependency. A linear dependency of the segregation velocity has been found on the shear rate in all these studies.

This dependency on the shear rate as well as the species concentration has been also confirmed for mixtures with same size but different density particles (Xiao et al. (2016); Fry et al. (2018); Jones et al. (2018); Fry et al. (2019)). By performing DEM simulations of quasi 2D heap flows, Xiao et al. (2016) obtained the linear dependence of the segregation velocity $v_{seg,i}$ on the local concentration of other species f_j and shear rate for binary mixtures differing in density. The authors proposed a correlation for the segregation velocity $v_{seg,i} = S_D \dot{\gamma} f_j$ as proposed by Fan et al. (2014) and Schlick et al. (2015a) in the case of size segregation. The segregation length scale S_D in different density mixtures was found to be proportional to the diameter d of the particles and logarithm of the density ratio ρ and was given as $S_D = d C_D \ln \rho$. The value of the empirical parameter (C_D) was estimated by linearly fitting the S_d vs. ρ data on a semi-log plot. Fry et al. (2018) modified this linear empirical segregation model to account for the effect of the confining pressure in addition to the local concentration and shear rate in

*Department of Chemical Engineering, Indian Institute of Technology Kanpur, Uttar Pradesh, 208016, India

Email address: anuragt@iitk.ac.in (Anurag Tripathi)

case of plane shear flows. In a followup study (Fry et al., 2019), the authors showed that the model is able to predict segregation in plane shear flow geometry for different densities as well as different size mixtures.

Jones et al. (2018) studied the segregation for a binary mixture due to density difference using DEM simulations in 2D bounded heap flow. The authors also investigated the size segregation of binary mixtures in the same geometry. Based on their findings, the authors revised the empirical model for the segregation velocity and proposed a quadratic dependence on the concentration along with the linear dependency on the shear rate. Duan et al. (2021) showed that the combined effect of size and density segregation in 2D quasi-heap flow can also be described well using the quadratic empirical model. The empirical parameters are found to be dependent on the size ratio as well as the density ratio. Duan et al. (2022) showed that this approach is also able to capture the segregation in a rotating tumbler.

Another promising approach to predict segregation is referred to as the particle force-based approach. By considering the forces on a high density intruder settling in a flowing granular medium, Tripathi and Khakhar (2013) proposed the particle force-based theory for predicting density segregation of binary mixtures in chute flow. In a recent study (Sahu et al., 2023), the particle force-based theory is extended for multi-component granular mixtures of different densities. This model is successfully able to capture the segregation in binary and multi-density mixtures. A similar approach is utilized by Tripathi et al. (2021) to obtain the theoretical expression for the segregation velocity of large size particles and predict the concentration profiles in binary size mixtures for periodic chute flows.

Both empirical as well as particle force-based approaches account for the effect of the species concentration and shear rate. However, the dependence on the species densities appears to be very different in these two approaches. While the particle force-based model suggests segregation velocity to be proportional to the density difference between the same size particles, the linear empirical model suggests that the density ratio of the species determines the segregation. A quick comparison of the particle force-based segregation velocity expression given by Duan et al. (2020) indeed suggests that the segregation parameter for the linear empirical model is proportional to the density difference and inversely proportional to the product of pressure and effective friction coefficient (i.e., the shear stress). Given the fact that the shear stress in the case of chute flows depends on the species concentration and inclination angle, the dependence of the empirical segregation parameter on these two can't be ruled out. Further, the particle force-based theory suggests strong inter-coupling of rheology and segregation with each other during the flow. The flow kinematics for systems starting from different initial configurations may be significantly different due to such inter-coupling of rheology and segregation. Since the empirical segregation parameters are obtained from the kinematics data during the flow evolution, the dependency of these parameters on flow configuration also remains to be explored. In this study, we compare the empirical and particle force-based segregation models in an identical geometry. Specifically, we chose periodic chute flow of different density

particles over a bumpy base and explore the effect of mixture composition, measurement time duration, density ratios at different inclination angles, and different initial configurations on the empirical segregation parameters.

The organization of the paper is as follows. Section §2 describes the simulation methodology for DEM simulations. Details of the calculation of the empirical segregation parameters estimation along with the effect of the measurement time and initial configuration are discussed in §3. This detailed analysis helps us identify the limitations of the empirical models and determine the best way to estimate the appropriate values of the empirical parameters. The theory utilizing the two empirical models to predict the concentration profile in the periodic chute is presented in §4. In addition, the predicted profiles are compared with the DEM simulation and particle force-based theory predictions in this section. The conclusions are presented in section §5.

2. Simulation methodology

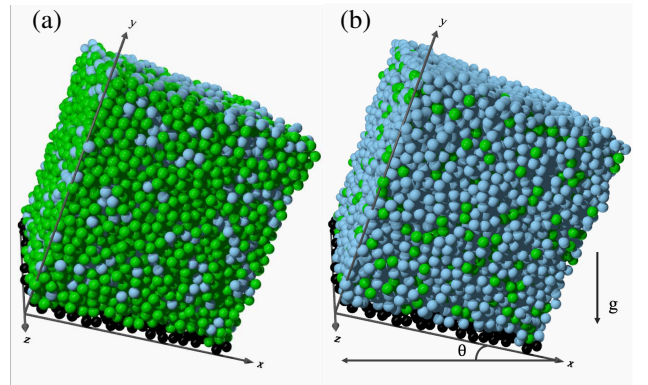


Figure 1: DEM simulation snapshots for binary granular mixture having (a) 20% and (b) 80% light particles with density ratio $\rho = 3.0$ flowing over an inclined plane at an inclination angle of θ . Green and blue particles represent the heavy and light particles, respectively. Black particles represent the rough bumpy base of thickness $1.2d$.

We simulate granular mixtures of different density particles, modelled as slightly inelastic and frictional spheres, flowing over a bumpy inclined surface. At the beginning of the simulation, the particles are positioned in such a way that their centers form a cubic lattice, ensuring that there is no contact between any pair of particles. Additionally, these particles are assigned random initial velocities. First, we settle the particles at a zero inclination angle and then increase the inclination to the desired angle. Figure 1 shows the uniformly mixed arrangement of high-density (green) particles of mass m_H and the light density (blue) particles of mass m_L for two different mixture compositions. The bumpy chute base, shown as black spheres in figure 1, is formed by taking a slice of $1.2d$ thickness from a randomly arranged, densely packed arrangement of spheres of the diameter of d . The simulation box has equal length and width of $20d$ in the flow (x) and the neutral (z) directions. The height of the simulation box in the y -direction is chosen to be sufficiently large in order to make sure that the particles never

reach the top surface to effectively mimic free surface flow. A total of 10000 flowing particles are simulated within the system so that the typical flowing layer height $H \approx 25d$. The simulations are performed for binary as well as ternary density mixtures over a wide range of compositions, and inclination angles. We consider three different initial configurations for density segregation: light near base, heavy near base, and well-mixed configuration.

The flow and segregation behavior of the mixtures is simulated using the Discrete Element Method (DEM) simulation. Following [Tripathi and Khakhar \(2011a\)](#), we use linear spring dashpot contact force model, and the Coulomb's friction law is used to limit the maximum permissible tangential force. The equations of motion are numerically integrated using a sufficiently small time step. Both gravity as well as inter-particle contact forces acting on the particles are accounted for to obtain the positions and velocities of every particle. All the particle properties used in the DEM simulations are identical to those used in [Tripathi and Khakhar \(2011a\)](#) and [Sahu et al. \(2023\)](#). Using the positions and velocities of the particles, all the relevant quantities of interest are calculated. Due to the periodic boundaries in the x and z direction, properties are obtained across different strips in the y direction. The sampling volume is taken as a strip of thickness d spanning the entire area of the simulation box in the $x - z$ plane. In order to get a good statistical average, the properties are averaged over a total of 20 time units obtained at regular intervals of 0.1 time unit.

Packing fraction of j^{th} species in the mixture is calculated as $\phi_j = (1/V) \sum_i \phi_{j,i}$, where $\phi_{j,i}$ is the volume fraction of i^{th} particle of the j^{th} species in the sampling volume V . The total packing fraction of the mixture is obtained as $\phi = \sum_j \phi_j$. The concentration of j^{th} species at any y location is obtained as

$$f_j = \frac{\phi_j}{\phi}. \quad (1)$$

Species velocity is calculated as,

$$\vec{v}_j = \frac{\sum \vec{c}_{j,i} \phi_{j,i}}{\sum \phi_{j,i}}, \quad (2)$$

where $\vec{c}_{j,i}$ is the instantaneous velocity of particle i belonging to species j . The average velocity of all the N particles partially or completely situated in the sampling volume V is calculated as $\vec{v} = \sum_{k=1}^N \phi_k \vec{c}_k$ where ϕ_k is the volume fraction of particle k in the sampling volume and \vec{c}_k is the instantaneous velocity of particle. The shear rate at each y location is calculated by numerically differentiating the velocity profile using forward difference method. Following [Fan et al. \(2014\)](#), [Xiao et al. \(2016\)](#), and [Jones et al. \(2018\)](#), the segregation velocity of j^{th} species $\vec{v}_{seg,j}$ is defined as the local velocity of species j with respect to mean flow \vec{v}_{mix} in the cases where contribution due to diffusional velocity is neglected, i.e.,

$$\vec{v}_{seg,j} = \vec{v}_j - \vec{v}_{mix}. \quad (3)$$

Data for the segregation velocity is obtained for each strip of thickness $1d$ across the entire flowing layer and is averaged over

an interval of 100 time units. Steady-state is characterized by a constant kinetic energy of the system and a constant height of the centre of masses of all the species in the mixture.

3. Calculation of empirical segregation parameter

A binary granular mixture flowing over an inclined surface is known to segregate in regions rich in one component. Previous studies (see [Fan et al. \(2014\)](#); [Schlick et al. \(2015a\)](#); [Xiao et al. \(2016\)](#); [Jones et al. \(2018\)](#); [Duan et al. \(2021\)](#)) use the empirical approach to predict the segregation due to size or density differences in free surface flows such as heap and rotating tumbler. All of these approaches utilize the flow and kinematics data starting from an initially well-mixed configuration for obtaining segregation parameters. Since this parameter determination utilizes the data during the flow evolution, the possibility of empirical parameters being dependent on the duration of observation can't be ignored. Hence, we performed DEM simulations and explored the effect of the observation time duration on the empirical parameter calculation. We consider a periodic chute flow simulation of a binary mixture having two different density particles. The usage of this setup provides a much better control over the inclination angle (and the shear rate) compared to other setups and facilitates investigation of the effect of the measurement time duration on empirical segregation parameters. Using this simple setup, we estimate the segregation time scale of the species using the data of centre of mass variation with the time. We first, discuss the duration of segregation for different compositions of binary density mixtures. Figure 2 shows the variation of the centre of mass (y_{com}) with time for three different mixtures. Figure 2a shows the data for a mixture having 20% light species ($f_L^T = 0.20$) whereas figures 2b and 2c show the data for $f_L^T = 0.50$ and $f_L^T = 0.80$ respectively. The data presented corresponds to a binary mixture with a density ratio of $\rho = 3.0$ flowing over an inclined plane at inclination $\theta = 25^\circ$. Following the studies mentioned in the beginning of this section, we start the simulations from an initial condition where the light and heavy particles are uniformly mixed. Hence, the centre of mass position of both the species at time $t = 0$ is nearly identical for all three cases. The particles are settled under the influence of gravity at zero inclination angle, resulting in a packing fraction close to a randomly closed-packed configuration. Shearing of such a closed-packed layer undergoes dilation as it starts to flow. Such a dilation at early times is observable in the inset of figures 2a, 2b, and 2c. Note that both heavy and light species exhibit a rise in the centre of mass position in the beginning due to the dilation of the layer. After an initial period of dilation, the centre of mass position of heavy species (green squares) decreases while that of light species (blue circles) increases with time. The y_{com} position of both the species becomes constant at larger times, indicating that steady-state segregation is achieved.

Ignoring the dilation for the initial times, the subsequent centre of mass variation can be captured very well using an exponential function. The following mathematical expression is

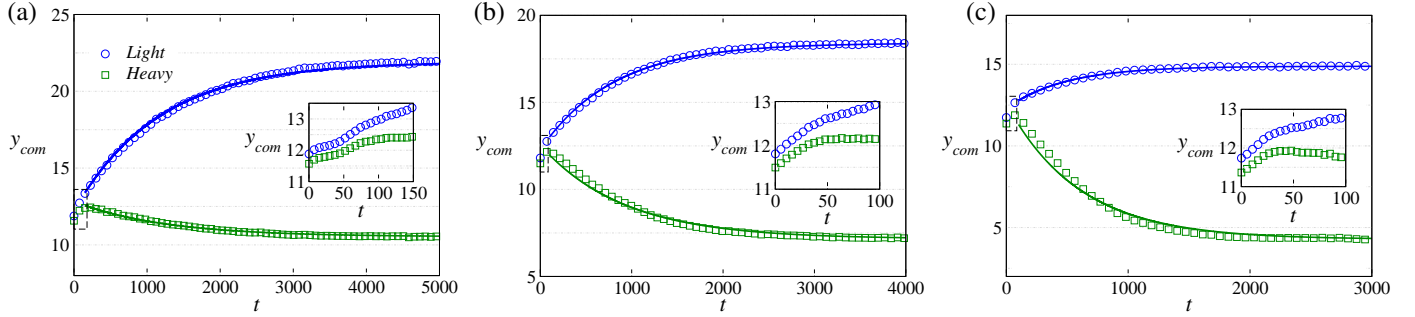


Figure 2: Centre of mass variation of light (blue circles) and heavy (green squares) species with time for a binary mixture having density ratio $\rho = 3.0$ starting from an initially well-mixed configuration. The composition of the light species in the mixture is (a) $f_L^T = 0.20$, (b) $f_L^T = 0.50$, and (c) $f_L^T = 0.80$. Symbols represent the DEM data and the lines are the exponential fits to the data.

used to fit the data shown in figures 2a-2c,

$$y_{com}(t) = y_{com}^0 + (y_{com}^\infty - y_{com}^0) \left(1 - e^{-(t-t_0)/\tau}\right). \quad (4)$$

In this expression, y_{com}^0 and y_{com}^∞ are the initial and final centre of mass positions of the species. τ is the time scale that characterizes the segregation phenomena and t_0 is the dilation time beyond which y_{com} of heavy species starts to decrease. A similar expression has been utilized by Staron and Phillips (2014) to calculate the segregation time scale. The exponential curve (shown using solid lines in figure 2) describes the data reasonably well for both the species for all three mixture compositions. The segregation time scale τ obtained by fitting equation 4 to the species centre of mass profiles is reported in table 1. Note that the segregation time scale is found to be different for the two species and varies with the composition of the mixture.

Segregation time scale	$f_L^T = 0.2$	$f_L^T = 0.5$	$f_L^T = 0.8$
Heavy species (τ_H)	1157	799	478
Light species (τ_L)	1237	916	599

Table 1: Segregation time scale for heavy and light species for three different mixture compositions shown in fig 2

Table 1 also shows that the time scale for both the species decreases with an increase in the composition of the light particles. Additionally, the time scale of the light species is found to be approximately 80 to 120 time units larger than that of heavy species. The average value of the time scales of the two species i.e., $\tau = (\tau_H + \tau_L)/2$ is taken as the mixture segregation time scale for further analysis.

3.1. Linear empirical models

Following Fan et al. (2014), Schlick et al. (2015a) & Xiao et al. (2016), we define the segregation velocity as the species velocity relative to the mixture velocity using equation 3. Using this definition, these studies have shown that the species segregation velocity scaled by the local shear rate i.e., $v_{seg,i}/\dot{\gamma}$, varies linearly with other species concentration f_j for bounded heap flows and rotating cylinders. Here, we report the data for the segregation velocity in periodic chute flow obtained from DEM

simulations in figure 3. These data correspond to a binary mixture density ratio $\rho = 3.0$ flowing at an inclination angle of $\theta = 25^\circ$. We consider the data for an observation duration of approximately two-time scales ($t_0 \leq t \leq 2\tau$). The data during the initial dilation period $t < t_0$ is not included. Following Xiao et al. (2016), the flow is started from an initially mixed configuration. The light species tends to rise towards the free surface, resulting in a positive segregation velocity. Conversely, heavy species move towards the base, leading to a negative segregation velocity.

Figure 3a shows the variation of the segregation velocity scaled by the shear rate $v_{seg,i}/\dot{\gamma}$ with the concentration of other species f_j . Different coloured symbols represent the local segregation velocity for different mixture compositions. Total five different mixtures compositions with $f_L^T = 0.2, 0.4, 0.5, 0.6,$ and 0.8 have been considered to ensure the full range of f_j from 0 to 1 in figure 3. The large scatter in the data points of figure 3a is substantially reduced by averaging it over bins of width $\Delta f_i = 0.02$ spanning over the entire concentration range. This data, shown in figure 3b, can be described very well using a straight line. The slope of the fitted line for the heavy species is $S_{D,H} = -0.023$ while that for the light species is $S_{D,L} = 0.023$. Note that the magnitude of slopes (termed as the segregation or percolation length scale in previous studies) for both species is identical. These results indicate that the segregation velocity scaling proposed by Xiao et al. (2016) for the density segregation holds true in the case of the chute flow as well. Thus, the segregation velocity of species i can be described using the following relation,

$$v_{seg,i} = S_D(i, j)\dot{\gamma}f_j. \quad (5)$$

Recall that the data reported in figure 3 correspond to an observation duration of approximately two-time scales. We now investigate the effect of the observation time on the empirical parameters. We first report the variation of the scaled segregation velocity with time. To explore this effect, we collect the scaled segregation velocity data for different time intervals. The data for the initial duration of layer dilation are discarded. Figure 4 illustrates the shear rate scaled segregation velocity for both the species for four distinct time intervals, each with a duration of 0.5τ . As before, the data are presented for a binary

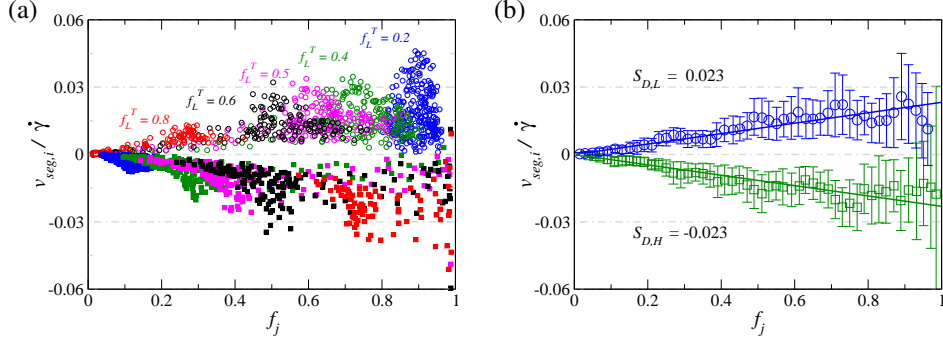


Figure 3: (a) DEM simulation data of shear rate scaled segregation velocity for light (circles) and heavy (squares) species of a binary mixture having density ratio $\rho = 3.0$ flowing over chute at inclination angle $\theta = 25^\circ$. Different colours correspond to different mixture compositions of light species in the range $f_L^T = 0.2$ to $f_L^T = 0.8$. (b) DEM simulation data for all the compositions averaged over every $\Delta f_i = 0.02$. Solid lines represent the linear fit to the averaged data.

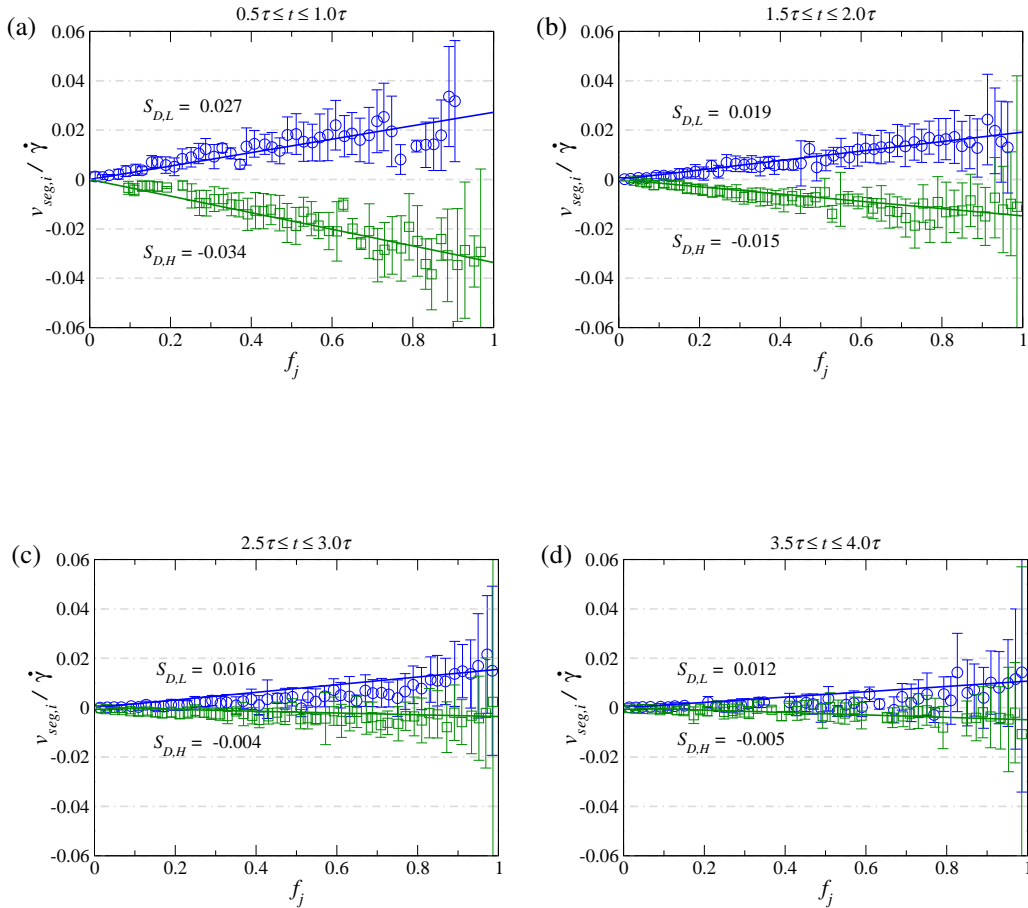


Figure 4: Dependency of the segregation parameter on the observation time duration (a) $0.5\tau \leq t \leq 1.0\tau$, (b) $1.5\tau \leq t \leq 2.0\tau$, (c) $2.5\tau \leq t \leq 3.0\tau$ and (d) $3.5\tau \leq t \leq 4.0\tau$. Blue symbols represent the light species, and green symbol represents the heavy species. Solid lines represent the linear fit to data reported for inclination angle $\theta = 25^\circ$ and density ratio $\rho = 3.0$.

mixture with $\rho = 3.0$ at 25° starting from the mixed configuration. The segregation velocity scaled by the shear rate as a function of concentration is shown for $0.5\tau \leq t \leq 1.0\tau$ in figure 4a, for $1.5\tau \leq t \leq 2.0\tau$ in figure 4b, for $2.5\tau \leq t \leq 3.0\tau$ in

figure 4c, and for $3.5\tau \leq t \leq 4.0\tau$ in figure 4d. Symbols represent the DEM data, and lines represent the linear fit to data. The slope of the fitted lines is mentioned for each time interval. The shear rate-scaled segregation velocities for both the species

exhibit higher values within the time range of $0.5\tau \leq t \leq 1.0\tau$. However, these scaled velocities decrease as time progresses. Notably, the values of $v_{seg,i}/\dot{\gamma}$ for both the species are significantly low during the time interval of $2.5\tau \leq t \leq 3.0\tau$ & $3.5\tau \leq t \leq 4.0\tau$. We find that the linear fit (equation 5) accurately describes the data for all the time intervals. However, the empirical parameters estimated from the linear fit to DEM data differ for different time intervals. The decreasing slope of fitted lines in figure 4 confirms that the species segregation velocity keeps decreasing with time and becomes nearly zero at steady state. This is in contradiction with the empirical models for segregation velocity. The linear empirical relation of equation 5 states that segregation velocity depends only on the shear rate $\dot{\gamma}$ and concentration of other species f_j . At steady state, the shear rate has a finite value, and except for the limiting cases of $f_i = 0$ & 1 , f_j is also non-zero. Therefore, according to equation 5 the segregation velocity should have a finite non-zero value at steady state. We consider this issue again later while discussing the role of diffusional velocity in estimation of segregation velocity using DEM. The time-dependent slope of scaled percolation velocity suggests that a time-averaged slope may be more appropriate for usage in equation 5. Hence we consider data from $t_0 \leq t \leq t_f$, where t_f ranges from 1τ to 2.5τ . For a time duration larger than 2.5τ , the segregation velocity becomes very small and remains practically indistinguishable from zero as the segregation process is around 95% complete. We find that even after averaging the data over various observation time frames, substantial differences remain noticeable and the value of S_D varies substantially for different values of t_f . Table 2 reports the absolute value of the segregation length scale empirically obtained from the DEM simulations for four different observation times. The segregation parameter has a negative value for heavy species and a positive value for light species.

Segregation parameter	τ	1.5τ	2τ	2.5τ
Heavy $ S_{D,H} $	0.031	0.027	0.023	0.020
Light $ S_{D,L} $	0.027	0.025	0.023	0.022
Average (S_D)	0.029	0.026	0.023	0.021

Table 2: Segregation length scale for heavy and light species for different observation time duration $t_0 \leq t \leq t_f$ for different values of t_f in the range τ to 2.5τ . Average value of the segregation parameter is calculated as $S_D = [|S_{D,L}| + |S_{D,H}|]/2$.

While the magnitude of segregation parameters of the two species are found to be reasonably close to each other, the values of the parameter seem to decrease as observation time increases. This decrease in the slopes is attributed to the fact that more data near the steady state are considered in the case of the higher value of t_f . It appears that a time duration of twice the segregation time scale is appropriate as it provides a long enough time window to capture most of the finite segregation velocity data without capturing the near-zero segregation velocity close to the steady state. Hence, we use the segregation parameter obtained over twice of segregation time scale (2τ) in the rest of the paper for the linear empirical model. Using the

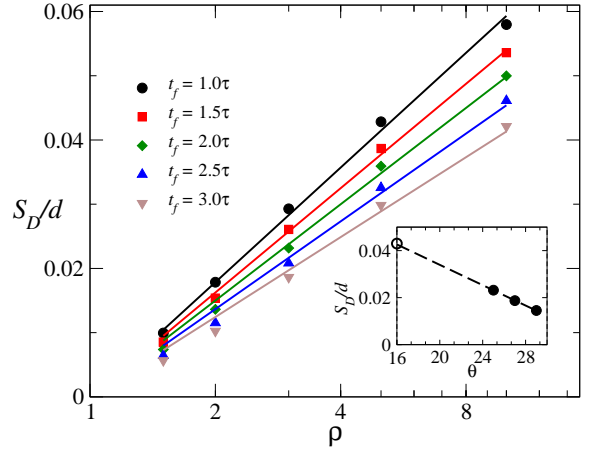


Figure 5: Variation of non-dimensional segregation parameter S_D/d with density ratio $\rho = \rho_H/\rho_L$ on a semi-log plot for binary mixture at $\theta = 25^\circ$ for different t_f .

linearly with the density ratio on the semi-logarithm scale for all five different time durations considered in this study. The data presented in this figure corresponds to a binary mixture flowing at an inclination angle of 25° starting from the mixed configuration. The data can be described using the relation $S_D(i, j)/d = C_D \ln(\rho_j/\rho_i)$ where C_D is an empirical parameter. This relation is identical to that reported by Xiao et al. (2016). However, the time duration for segregation velocity measurement has not been mentioned by the authors. Our results show that the value of empirical parameter C_D (i.e the slope of fitted lines in figure 5) decreases by almost 23% by increasing the time duration from 1τ to 3τ . Figure 5 inset shows the data for S_D/d variation at different inclination θ for a binary mixture of density ratio $\rho = 3.0$. Evidently, the S_D/d value increases with decreasing the inclination angle θ . The dashed line shows the extrapolated line for lower inclination angles. Xiao et al. (2016) reported that the segregation parameter S_D is 0.15 mm for the binary mixture having identical size particles of diameter $d = 3$ mm and density ratio $\rho = 3.0$ flowing at inclination angle $\theta = 16^\circ$ (Figure 7 of their study). Notably, the dimensionless value of $S_D = 0.05$ is found to be close to our extrapolated value of 0.043. Based on their results, we use the value of C_D corresponding to a measurement time of 2τ while using the linear empirical segregation model and predict the theoretical concentration profile for binary as well as multi-component mixture flowing over a chute in section §4.

3.2. Quadratic empirical model

Linear empirical models (Fan et al. (2014), Schlick et al. (2015a), and Xiao et al. (2016)) describing the segregation due to either size differences or density differences utilize equation 3 to measure the segregation velocity from DEM simulations. A recent study by Duan et al. (2021) dealing with the combined size and density segregation suggests that this method of measurement of the segregation velocity using DEM

simulations is not appropriate. The authors revise the method to calculate segregation velocity and incorporate the presence of the diffusional velocity using the following expression

$$v_{seg,i} = v_i - v_{mix} + \frac{1}{f_i} D \frac{\partial f_i}{\partial y}. \quad (6)$$

The rationale for the addition of the last term can be understood by multiplying the above equation with f_i . The equation then states that the flux of the species i in the y -direction $f_i v_{seg,i}$ is due to the combined effect of convective flux $f_i(v_i - v_{mix})$ and the diffusion flux $D \partial f_i / \partial y$. In the case of significant size or density differences between the species, the contribution of the convective flux is much larger than the diffusive flux, and hence ignoring the latter leads to little error. It is important to note that the above discussion pertains to the empirical measurement of the segregation velocity using the DEM simulations. The previous studies used only the relative velocity of the species with respect to the mixture velocity to measure the segregation velocity at any location. The revised method accounts for the correction due to the presence of diffusion. Given the focus of the present study, we investigate the role of convective and diffusional contributions to the segregation velocity calculations in detail.

To better understand this, we consider a system in which only diffusion is present, and the segregation effect is absent. We consider mono-disperse particles, identical in all aspects but tagged as two different species flowing over an inclined surface. The particles in the lower portion are tagged as species 1 and the upper portion particles are tagged as species 2. In this case, the sizes and densities of both species are equal, and hence we expect the segregation velocity to be zero and only diffusion velocity to be present. The figure 6a and 6b show the shear rate scaled segregation velocity $\frac{v_{seg,i}}{\dot{\gamma}}$ where $v_{seg,i}$ is computed using equation 6, as well as shear rate scaled diffusional velocity $\frac{v_{diff,i}}{\dot{\gamma}}$ (where $v_{diff,i} = \frac{1}{f_i} D \frac{\partial f_i}{\partial y}$). Filled symbols represent the diffusional velocity and empty symbols represent the segregation velocity. Evidently, we find that the segregation velocity using equation 6 is close to zero at all times. This indeed appears to be the case for not only the first two time scales (figure 6a) but also the next two time scales (figure 6b). Diffusional velocity, represented with filled symbols, is noticeable only for initial times $t_0 \leq t \leq 2\tau$ (figure 6a). It becomes close to zero for time $2\tau \leq t \leq 4\tau$ as both identical species mix together, and the concentration gradient becomes zero (figure 6b). As in figure 3, the data shown in figure 6 are obtained by considering five different mixtures of composition 20%, 40%, 50%, 60% and 80% of one of the species. In figures 6a and 6b, we also use the data for 10% and 90% compositions to obtain the entire range of concentration from 0 to 1.

Figure 6c & 6d show the diffusional velocity along with the segregation velocity (given by equation 6), both scaled by the shear rate. The data are shown for a binary mixture of density ratio $\rho = 3.0$ flowing at $\theta = 25^\circ$. During the $t_0 \leq t \leq 2\tau$ time interval, the diffusional velocity is found to be close to zero (figure 6c) since we start from a uniformly mixed configuration. Hence the segregation velocity arises primarily due to the

convective motion of the species relative to the mixture. Figure 6d shows the same data for a time interval ranging from two to four time scales, i.e., $2\tau \leq t \leq 4\tau$. In contrast to figure 6c, the diffusional velocities of both species appear to be almost equal to the segregation velocities confirming that the convective contribution $v_i - v_{mix}$ (not shown here) to the segregation velocity is negligible. Figures 6e & 6f, show the same data for a mixture starting from a completely segregated initial configuration with heavy particles near the base. As before, figure 6e shows the data for time up to two-time scale, while figure 6f shows the data for a time interval ranging from two to four time scales. In contrast to figure 6c & 6d for mixed configuration, it is evident that convective flux is negligible not only for time $2\tau \leq t \leq 4\tau$ but also for time $t_0 \leq t \leq 2\tau$.

The observations made in figure 6c-6f can be understood as follows. Starting from a well-mixed configuration, the concentration gradient $\partial f_i / \partial y$ and hence diffusional contribution remains close to zero (figure 6c) initially, and the segregation occurs entirely due to the relative motion of the species with respect to each other. This relative motion leads to the build-up of concentration gradient $\partial f_i / \partial y$ across the layer, which leads to increasing importance of the diffusional contribution at later times (figure 6d). In the case of starting from an initial configuration of segregated case, the high concentration gradients exist since beginning and hence the behaviour in figure 6e is similar to figure 6d. As the final steady state configuration also has heavy particles concentrated near the base, no difference in the figure 6e and figure 6f noticeable. Results shown in figure 6c-6f confirm that the assumption of diffusional contribution being small in case of density segregation is not correct and the relative importance of the diffusion flux and convective flux depends upon the initial configuration and may also change as the flow evolves.

Figure 7 shows the variation of the shear rate scaled segregation velocity with the concentration of other species for the initially mixed configuration. The segregation velocity $v_{seg,i}$ is computed using equation 6 by utilizing the data for time duration $2\tau \leq t \leq 4\tau$. Green square symbols represent the DEM data for heavy species, and blue circles represent the light species. Figures 7a - 7b show the effect of density ratio on shear rate scaled velocity variations at inclination angle $\theta = 25^\circ$. Figure 7a corresponds to density ratio $\rho = 1.5$ and 7b corresponds to $\rho = 3.0$. Figure 7c shows data for density ratio $\rho = 3.0$ at $\theta = 29^\circ$. Comparing the magnitude of $v_{seg,i} / \dot{\gamma}$ in figures 7a and 7b, it is clear that it increases with increase in the density ratio. Comparison of figures 7b and 7c shows the effect of inclination angle at a given density ratio $\rho = 3.0$. An increase in the inclination angle from $\theta = 25^\circ$ to $\theta = 29^\circ$ leads to a slight reduction in the shear rate scaled segregation velocity. The solid lines correspond to a quadratic fit confirming that the shear rate-scaled segregation velocity exhibits a quadratic variation with concentration. We use the segregation velocity relation proposed by Jones et al. (2018) and Duan et al. (2021) to fit the DEM data shown in figure 7. The authors used the following expression relating shear rate segregation velocity with concentration,

$$v_{seg,i} / \dot{\gamma} = df_j(A_{ij} + B_{ij}f_j), \quad (7)$$

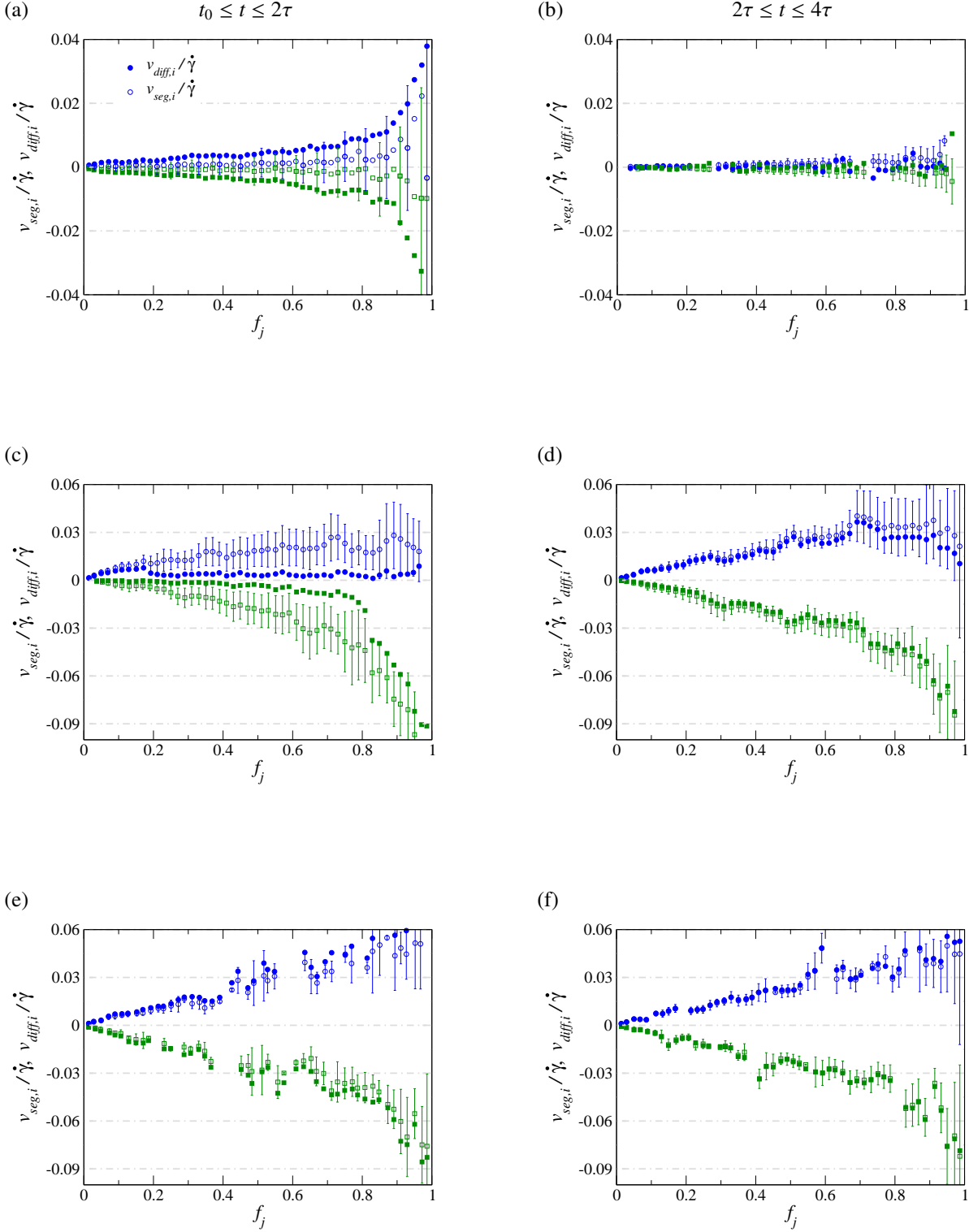


Figure 6: Shear rate scaled segregation velocity (empty symbols) and diffusional velocity (filled symbols) with the concentration of other species in a mixture for two different time durations $t_0 \leq t \leq 2\tau$ (left column) and $2\tau \leq t \leq 4\tau$ (right column). Results for the same size and same density particle mixture are shown in (a) and (b). Results for a binary mixture of density ratio $\rho = 3.0$ starting from a mixed initial configuration are shown in (c) and (d). (e) and (f) show data for heavy near base initial configuration. Blue circles, and green squares represent the light and heavy species respectively.

where A_{ij} and B_{ij} are the empirical parameters. We report the values of these parameters for both species in table 3. We observe that the magnitudes of A_{LH} and B_{LH} for light species in-

crease with increase in the density ratio, and decreases with increase in the inclination angle. This is consistent with the findings of Jones et al. (2018) and Duan et al. (2021). From these

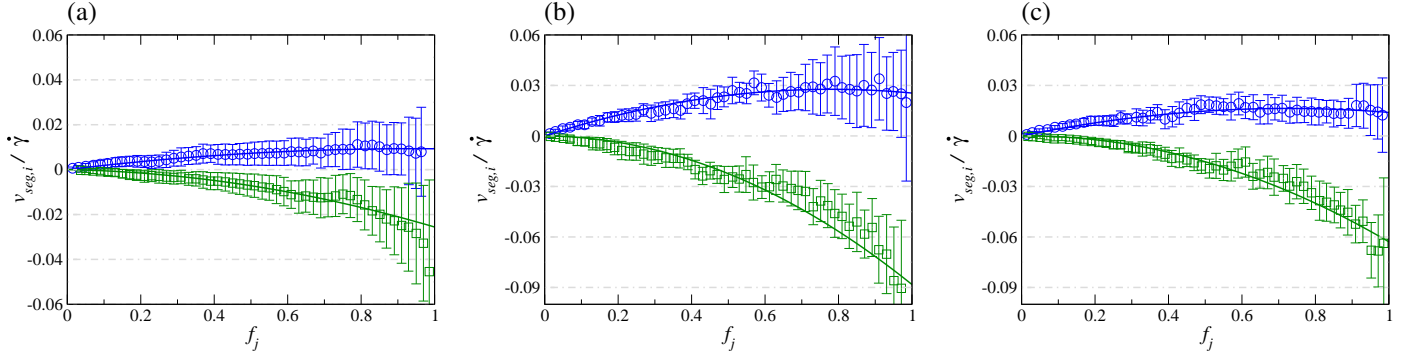


Figure 7: Shear rate scaled segregation velocity variation with concentration for binary mixture having for density ratio (a) $\rho = 1.5$; (b) $\rho = 3.0$ at inclination angle $\theta = 25^\circ$, (c) $\rho = 3.0$ at inclination angle $\theta = 29^\circ$. Blue symbols represent the light species, and green symbol represents the heavy species. Blue and green solid lines represent the quadratic fit to the data $v_{seg,i}/\dot{\gamma} = df_j(A_{ij} + B_{ij}f_j)$.

results, we conclude that quadratic variation of shear rate scaled segregation velocity with concentration is indeed observed in the case of chute flow as well. However, the dependency on inclination angle θ is also observable since the parameters A_{ij} & B_{ij} for $\theta = 25^\circ$ & $\theta = 29^\circ$ differ substantially from each other. While increase in θ leads to higher shear rates, the model is unable to account for this dependency on θ using the shear rate scaling.

Density ratio (ρ)	inclination angle (θ)	A_{LH}	B_{LH}	A_{HL}	B_{HL}
$\rho = 1.5$	$\theta = 25^\circ$	0.022	-0.013	-0.001	-0.026
$\rho = 3.0$	$\theta = 25^\circ$	0.082	-0.054	-0.003	-0.083
$\rho = 3.0$	$\theta = 29^\circ$	0.047	-0.028	-0.004	-0.057

Table 3: Empirical parameters for the species obtained using quadratic fitting (equation 7) of $v_{seg,i}/\dot{\gamma}$ vs f_j data for binary mixture, shown in figure 7.

We next explore the effect of initial configuration on the empirical parameters estimated using the two segregation models. We estimate the empirical parameters for binary granular mixtures starting from two different initial configurations. We follow the terminology used by [Sahu et al. \(2023\)](#). The configuration with the heavy species initially concentrated near the base is referred to as the heavy near base (HNB) case. A snapshot for the HNB case is shown in figure 8a. The light near base (LNB) case, depicted in figure 8b, consists of the low-density species concentrated entirely near the base and the high-density species entirely near the free surface. In figures 8a and 8b, the green spheres represent the high-density particles, and blue spheres represent the low-density particles. The inclined surface has an angle of 25° and the mixture has a density ratio $\rho = 3.0$. Figures 8c and 8d show the variation of $v_{seg,i}/\dot{\gamma}$ with the concentration of other species f_j for HNB and LNB cases, respectively for the linear empirical model. $v_{seg,i}$ (computed using equation 3) divided by the shear rate is plotted with f_j by utilizing the data for observation time up to twice the segregation time scale (2τ). The magnitude of $v_{seg,i}/\dot{\gamma}$ for both HNB and LNB case are different from that for the mixed state (shown in figure 3b). Since the HNB configuration is already close to the final segregated

state, very low values of the percolation velocities are obtained. The shear rate scaled segregation velocity for the LNB case is approximately 10 times higher than the HNB case. Using linear fit to get the empirical parameters for linear model appears to differ by nearly an order of magnitude for the two configurations. Further, the data for the LNB case does not seem to be described well using the linear fit for $f_j \geq 0.50$. These results confirm the dependency of initial configuration on the parameter estimation using the linear empirical model.

Figure 8e shows the $v_{seg,i}/\dot{\gamma}$ calculated using equation 6 and relate it with f_j using the quadratic empirical approach for HNB case. Figure 8f shows the same data for the LNB case. In both the figures, we employ data beyond twice the segregation time scale 2τ (i.e., $2\tau \leq t \leq 4\tau$). The magnitude of the $v_{seg,i}/\dot{\gamma}$ in both the configurations is found to be comparable to each other as well as to the mixed case discussed in figure 7b. Fitting equation 7 to the data reveals that the values of the empirical parameters A_{ij} and B_{ij} for both species are slightly different from each other. However, the predicted segregation velocity seems to differ only for large values of f_j . Thus we can conclude that the initial configuration doesn't play as significant role in empirical parameter estimation in the case of the quadratic empirical model as in the linear case.

4. Comparison of empirical and particle force-based segregation models

The studies for heap flow and rotating cylinders suggest that the empirical models of segregation velocity coupled with the convection-diffusion-segregation equation can predict the concentration profile in good agreement with DEM simulations and experiments. In this section, we explore the applicability of the empirical approach for periodic chute flows. We solve the steady state 1D diffusion-segregation equation ([Tripathi and Khakhar, 2013](#); [Sahu et al., 2023](#)) along with the momentum balance equations and the inertial number-based rheology following the approach [Tripathi and Khakhar \(2011b\)](#) and [Sahu et al. \(2023\)](#). Both empirical as well as particle force-based segregation models have been utilized to predict the steady-state concentration profiles theoretically.

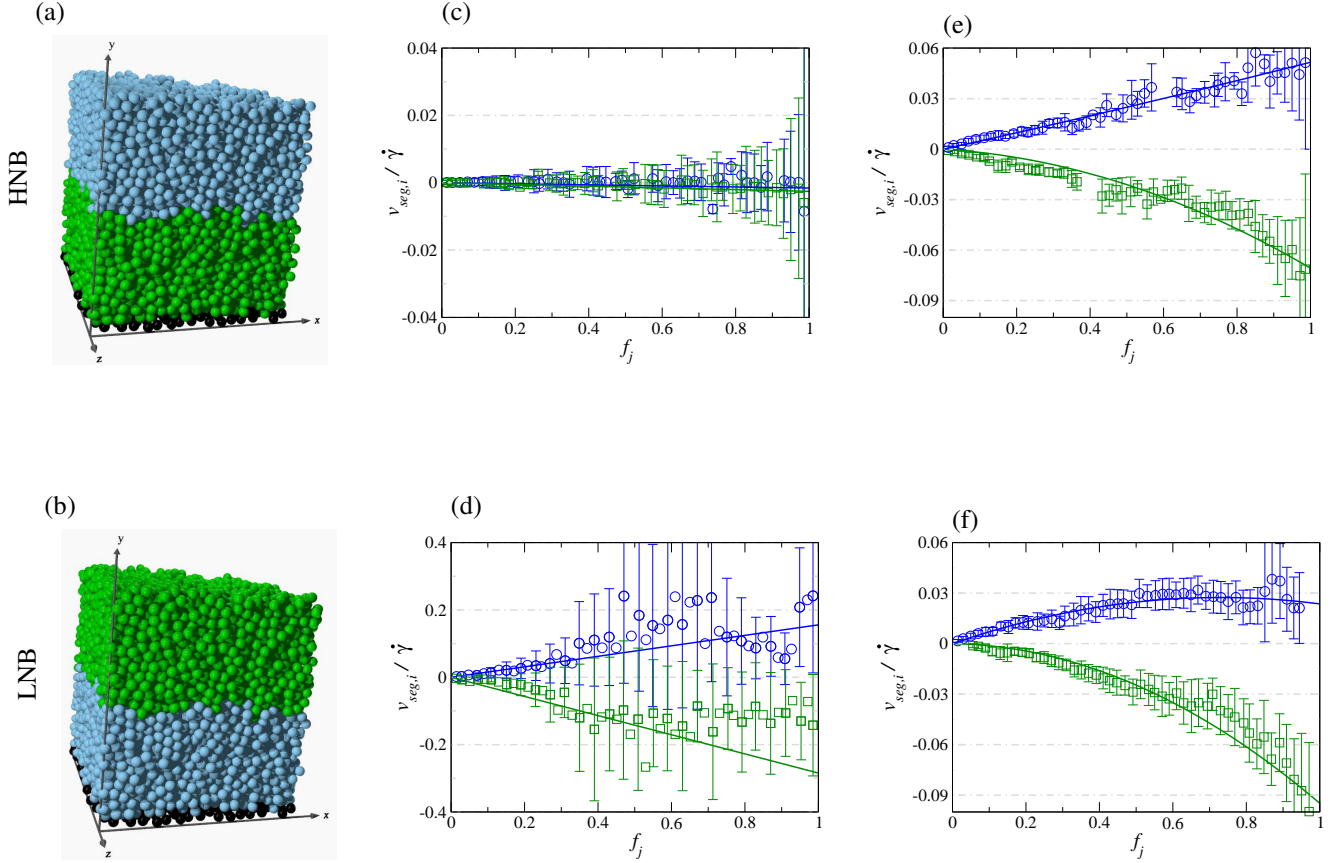


Figure 8: Snapshots showing an initial configuration of (a) Heavy near base (HNB) case and (b) Light near base (LNB) case for a binary mixture of equal compositions of each species at an inclination angle $\theta = 25^\circ$ with density ratio $\rho_H : \rho_L = 3 : 1$. Black spheres represent the bumpy base. Shear rate scaled segregation velocity (neglecting diffusional velocity) used in linear empirical model for the (c) HNB case and (d) LNB case (error bars shown only for alternate data points for the sake of clarity). The data are taken for $t_0 \leq t_f \leq 2.0\tau$. Shear rate scaled segregation velocity (accounting for diffusional velocity) used in quadratic empirical model for the (e) HNB case and (f) LNB case. The data are taken for $2.0\tau \leq t_f \leq 4.0\tau$.

4.1. Theory

We consider a fully developed flow over an inclined surface which is simulated by employing a periodic chute in the DEM simulations. For this system, the concentration gradient along the flow direction vanishes, and hence, the convection term in the convection-diffusion-segregation equation (Xiao et al. (2016); Duan et al. (2021)) becomes zero. At steady state, the transient term also vanishes, and the equation reduces to a simple flux balance equation for the species (Tripathi and Khakhar (2013), Sahu et al. (2023)),

$$\Phi_{seg,i} + \Phi_{diff,i} = 0. \quad (8)$$

Using the expression for the diffusion flux $\Phi_{diff,i} = -D \frac{\partial f_i}{\partial y}$ and segregation flux $\Phi_{seg,i} = v_{seg,i} f_i$, we obtain an ordinary differential equation

$$v_{seg,i} f_i - D \frac{df_i}{dy} = 0, \quad (9)$$

where $v_{seg,i}$ is the segregation velocity and D is the diffusivity. Several studies, including Fan et al. (2014), Schlick et al. (2016), Deng et al. (2018), and Deng et al. (2020) utilized a constant value of the diffusivity in the theoretical predictions. Utilizing a constant diffusivity in the empirical approach to solve

equation 9 would require the knowledge of $\dot{\gamma}$ due to the dependence of percolation velocity $v_{seg,i}$ on the local shear rate $\dot{\gamma}$. For this, one needs to incorporate information about flow kinematics for predicting segregation. DEM simulations confirm that the average value of diffusivity depends on inclination angle θ (see Figure 8 by Tripathi and Khakhar (2013)) and hence separate diffusivity values need to be used for each inclination angle to get reasonable predictions. Table S1 in the appendix shows that a very weak dependency of the average diffusivity on the mixture composition is observed. However, the average diffusivity values for $\theta = 25^\circ$ and $\theta = 29^\circ$ differ significantly from each other. Figure S1 confirms that the predictions using the particle force-based theory also differ significantly if the diffusivity value corresponding to the particular inclination angle is not used.

Variation of the diffusivity with the shear rate has been reported by many researchers (Bridgwater et al. (1985); Utter and Behringer (2004); Tripathi and Khakhar (2013); Fan and Hill (2015); Fry et al. (2019); Sahu et al. (2023)). It is observed that the diffusivity (D) varies linearly with the shear rate, $D = b\dot{\gamma}d_{mix}^2$, where d_{mix} is the local volume average diameter. b is a constant parameter obtained using DEM simulation. We use $b = 0.041$, obtained by Tripathi and Khakhar (2013) and

Sahu et al. (2023) in the case of density segregation. For different density and same size particle mixtures, $d_{mix} = d$. By utilizing the variation of diffusivity on the local shear rate and concentration using relation $D = b\dot{\gamma}d_{mix}^2$, the need for the detailed information about flow kinematics is eliminated, and the equation can be solved analytically. The usage of diffusivity linearly scaling with the shear rate automatically takes care of diffusivity variation with inclination and hence should be preferred. In this study, we account for the shear rate dependence of the diffusivity and use this relation to obtain analytical solutions of equation 9 for both linear and quadratic empirical relation of $v_{seg,i}$. For the linear segregation model (given by equation 5) equation 9 simplifies to

$$b\dot{\gamma}d^2 \frac{df_i}{dy} = S_D(i, j)\dot{\gamma}f_j f_i. \quad (10)$$

Using $f_j = 1 - f_i$ for the binary mixture case and integrating equation 10 with boundary condition $f_i(y=0) = f_{i0}$, we get

$$f_i = \frac{f_{i0} \exp\left(\frac{S_D}{bd^2}y\right)}{1 - f_{i0} \left(1 - \exp\left(\frac{S_D}{bd^2}y\right)\right)}. \quad (11)$$

Equation 11 describes the variation of species concentration f_i with y across the layer using an explicit function for the linear empirical segregation model. On the other hand, using quadratic empirical relation (given by equation 7) in the flux balance equation (equation 9), we get

$$b\dot{\gamma}d^2 \frac{df_i}{dy} = \dot{\gamma}df_j(A_{ij} + B_{ij}f_j)f_i, \quad (12)$$

where $f_j = 1 - f_i$ is the concentration of other species. Integrating equation 12 with boundary condition $f_i(y=0) = f_{i0}$, we get an implicit equation for f_i given as

$$y = \frac{1}{bd} \left[\frac{B_{ij}}{A_{ij}(A_{ij} + B_{ij})} \log\left(\frac{A_{ij} + B_{ij} - B_{ij}f_{ij}}{A_{ij} + B_{ij} - B_{ij}f_{i0}}\right) + \frac{1}{A_{ij} + B_{ij}} \log\left(\frac{f_i}{f_{i0}}\right) - \frac{1}{A_{ij}} \log\left(\frac{1 - f_i}{1 - f_{i0}}\right) \right]. \quad (13)$$

Both equation 11 and equation 13 require the knowledge of f_{i0} i.e., the value of f_i at $y = 0$ to predict the concentration variation across the layer. This value, however, is not known a priori. In order to obtain the value of f_{i0} , we make use of the overall species balance across the flowing layer. For this mass balance, the depth-averaged concentration of the species in the layer must be equal to the total mixture composition f_i^T . In other words, the integral of the species concentration $f_i(y)$ across the flowing layer divided by the layer thickness H must be equal to the total composition of the species i , i.e.,

$$\frac{1}{H} \int_0^H f_i dy - f_i^T = 0. \quad (14)$$

Equation 14 can be solved analytically for the linear empirical model. Specifically, we use equation 11 in the equation 14 to

get

$$\frac{1}{H} \int_0^H \frac{f_{i0} \exp\left(\frac{S_D}{bd^2}y\right)}{1 - f_{i0} + f_{i0} \exp\left(\frac{S_D}{bd^2}y\right)} dy = f_i^T. \quad (15)$$

Equation 15 can be easily integrated to get the value of the unknown concentration f_i at $y = 0$, i.e., f_{i0}

$$f_{i0} = \frac{1 - \exp\left(\frac{S_D}{bd^2}Hf_i^T\right)}{1 - \exp\left(\frac{S_D}{bd^2}H\right)}. \quad (16)$$

In the case of the quadratic model analytical solution for f_{i0} can't be obtained. In this case, we obtain f_{i0} iteratively by following the approach used by the Tripathi and Khakhar (2013). We start by assuming an initial guess value of f_{i0} at $y = 0$ and solve the equation 13 to compute the species concentration f_i across the layer height H . Subsequently, we numerically calculate the *LHS* of equation 14, which should be equal to 0 to ensure the species mass balance. Numerically this condition is assumed to be satisfied if the absolute value of the *LHS* of equation 14 turns out to be less than the tolerance value. In this work, we use a tolerance value of 10^{-4} . Given that $f_i^T \geq 0.1$, this tolerance value leads to less than 0.1% error in the mass balance. If this condition is not satisfied, we update the value of f_{i0} by a small increment (or decrement) of $\Delta f_{i0} = 10^{-5}$. We repeat this process until the tolerance criteria is satisfied to obtain f_{i0} .

While the flux balance equations for the binary mixture case (equations 10 and 13) can be solved analytically, the equations for mixtures with more than two components require a numerical solution. We note that the linear empirical model has been extended for multi-component mixtures differing in density by Deng et al. (2018). The particle force-based segregation model has also been extended for multi-component mixtures by Sahu et al. (2023). However, the quadratic empirical model has not been extended for multi-component density segregation. Studies involving multi-component mixtures differing in size (Gray and Ancy 2011; Deng et al. 2019) as well density (Deng et al. 2018; Sahu et al. 2023) suggest that the segregation flux $\phi_{seg,i}^{Multi}$ of a species i in a multi-component mixture of N species can be written as the summation of the binary segregation fluxes with respect to all the other species in the mixture, i.e., $\phi_{seg,i}^{Multi} = \sum_{j=1, j \neq i}^N \phi_{seg,i}^{Binary}(i, j)$. The species flux balance (equation 8) for multi-component mixtures can be written as

$$-D \frac{\partial f_i}{\partial y} + \sum_{j=1, j \neq i}^N \phi_{seg,i}^{Binary}(i, j) = 0. \quad (17)$$

Employing the linear empirical model given by equation 5, i.e., $v_{seg,i} = S_D(i, j)\dot{\gamma}f_j$ and $\phi_{seg,i} = v_{seg,i}f_i$, we have $\phi_{seg,i}^{Binary}(i, j) = S_D(i, j)\dot{\gamma}f_j f_i$. Since $D = b\dot{\gamma}d_{mix}^2$, the dependency on the shear rate is eliminated for the empirical model and equation 17 simplifies to

$$\frac{\partial f_i}{\partial y} = \frac{1}{bd^2} \sum_{j=1, j \neq i}^N S_D(i, j)f_j f_i. \quad (18)$$

In the case of the quadratic empirical model $\phi_{seg,i}^{Binary} = (A_{ij} +$

$B_{ij}f_j)f_jf_i$ and the equation 17 simplifies to

$$\frac{\partial f_i}{\partial y} = \frac{1}{bd} \sum_{j=1, j \neq i}^N (A_{ij} + B_{ij}f_j)f_i f_j. \quad (19)$$

Equations 18 and 19 represent the spatial variation of species i in a mixture of N components. Hence i can take any value from 1 to N . Since $\sum_{i=1}^N f_i = 1$, we get $N - 1$ inter-coupled, non-linear differential equations that need to be solved simultaneously. We solve equations 18 and 19 numerically using *ode45* in MATLAB with an initial guess of f_{i0} by following the Algorithm 1. The iterative method is employed in the quadratic approach to obtain f_{i0} . The empirical parameters are estimated for different combinations of density ratios. In the linear empirical approach, the relationship of S_D with density ratios $S_D(i, j) = C_D d \ln \rho_j / \rho_i$ facilitates solution for any generic pair of ρ_i and ρ_j . However, for the quadratic model, parameters A_{ij} and B_{ij} are obtained for a particular density ratio.

Note that it is possible to obtain the relation of quadratic empirical model parameters A_{ij} and B_{ij} with density ratio as reported by Duan et al. (2021). However, given the focus of the paper, we use the A_{ij} and B_{ij} for the specific combinations of density ratios corresponding to the binary mixture of the same density ratio. Using the equations described above, we obtain the concentration profiles of species across the layer for empirical segregation models (linear as well quadratic). The predictions for the particle force-based theory for binary mixtures are done following the approach of Tripathi and Khakhar (2013). Specifically, we use the algorithm given in Table 5 of their work. For ternary mixtures, we follow algorithm given by Sahu et al. (2023). We utilize the same set of parameters as used in these references and the interested reader is encouraged to look at these references for more details.

4.2. Comparison of theoretical predictions

Next, we compare the theoretical prediction using the linear empirical model of Xiao et al. (2016) and quadratic empirical model of Duan et al. (2021) with the particle force-based theory proposed by Tripathi and Khakhar (2013) and Sahu et al. (2023). As shown in section §3, the empirical parameters for the mixed configuration obtained using the linear segregation model are more reliable in comparison to LNB and HNB configurations. Hence, we utilize the empirical parameters obtained for the mixed configuration in these theoretical predictions. While the empirical parameters obtained using the quadratic approach are found to be relatively less dependent on the initial configuration, we use the parameters for mixed configuration for quadratic model as well.

Figures 9a - 9d show the comparison of the theoretical predictions using linear (dashed lines) and quadratic (dotted lines) empirical models. The steady-state DEM simulation data are shown as symbols for comparison. The concentration profiles of light species are shown for the three different mixture compositions of light species $f_L^T = 0.20$ (black), 0.50 (green) and 0.80 (brown). Figure 9a, 9b, 9c, & 9d show the results for density ratio $\rho = 1.5, 2.0, 3.0$ and 5.0 respectively using the empirical

model. Figure 9e, 9f, 9g, and 9h show the predictions using the particle force-based theory using solid lines for the same density ratios. Thus each column in figure 9 corresponds to a particular density ratio.

Let us first consider mixtures with the composition of light species $f_L^T = 0.20$. Figure 9a shows that the predictions using the linear segregation model (black dashed line) show significant differences with DEM data (black circles) at density ratios $\rho = 1.5$. Similar behaviour is observed for $\rho = 2.0$ (figure 9b), $\rho = 3.0$ (figure 9c), and $\rho = 5.0$ (figure 9d). However, these differences in the predictions appear to be decreasing with the increase in the density ratio. On the other hand, the quadratic empirical model (black dotted line) shows relatively small differences and seems to be describing the simulation data comparatively better for the density ratio of $\rho = 1.5$ for $f_L^T = 0.20$ (figure 9a). At higher density ratios of $\rho = 2.0, \rho = 3.0$, and $\rho = 5.0$, the differences between data & theory get substantially reduced, and the black dotted line follows the black circles very well, indicating that the quadratic empirical segregation model predicts segregation very well for a dilute mixture of light particles for $\rho \geq 2.0$. For $f_L^T = 0.50$, predictions using the quadratic approach match better with the DEM results in comparison to linear empirical model for higher density ratios. At lower density ratios, the two models appear to be similar in their agreement with the DEM simulation data. For the mixtures having high composition of light species $f_L^T = 0.80$, the predictions using the linear empirical model (dashed lines) match with DEM data very well. However, the predictions using the quadratic empirical model show noticeable differences at low density ratios. The deviation between the data (symbols) and dotted lines decreases with increase in ρ . Theoretical predictions using the particle force-based theory, shown in figures 9e, 9f, 9g, and 9h, on the other hand are found to match well with DEM data across the entire composition range and various density ratios. In order to quantify the deviations of the theoretical predictions with the simulation data, we compute the root mean square deviation (RMSD) and compare these three segregation models, namely the particle force-base model, and the linear and quadratic empirical segregation model. The RMSD value, calculated as

$$RMSD_j = \sqrt{\frac{\sum_{i=1}^{N_{bin}} [f_j^{th}(y_i) - f_j^{DEM}(y_i)]^2}{N_{bin}}}, \quad (20)$$

quantifies the deviation of the theoretical predictions of the concentration profile $f_j^{th}(y)$ obtained using the segregation model from that of DEM simulations data $f_j^{DEM}(y)$ for the j^{th} species in the mixture. Here, N_{bin} denotes the number of DEM data points in the concentration profile obtained from DEM simulations. Since we use bin sizes of $1d$ thickness to obtain DEM simulations, N_{bin} equals $H/d = 24$. Figure 10 shows the RMSD values for different composition mixtures at density ratio $\rho = 1.5, \rho = 2.0, \rho = 3.0$, and $\rho = 5.0$ shown in figures 10a, 10b, 10c, and 10d respectively. As before, the dashed and dotted lines correspond to the linear and the quadratic empirical models, respectively. The solid lines correspond to the particle force-based theory. Figures 10a - 10d show that for mix-

Algorithm 1: Algorithm used for predicting concentration of N component mixture using empirical segregation model

```

for  $i \leftarrow 1$  to  $N - 1$  do
  | Initialize  $f_i(y) = f_i^T$  at all  $y$ ;
  | Initialize  $f_{i0}$ ;
end
define  $error = 1$ ;  $tolerance = 10^{-4}$ ;  $\Delta f_0 = 10^{-5}$ ;
while  $error > tolerance$  do
  | for use in ODE45 solver;
  | for  $i \leftarrow 1$  to  $N - 1$  do
  | | Define  $f_i(y)$  in symbolic form;
  | end
  | for  $i \leftarrow 1$  to  $N - 1$  do
  | | Solve equations 18 (19) using ode45 with boundary condition  $f_i(y = 0) = f_{i0}$  to compute new  $f_i(y)$ ;
  | | Compute difference between the calculated and actual total composition of the species using 14;
  | end
  | Compute  $f_N = 1 - \sum_{i=1}^{N-1} f_i$ ;
  | Define  $error = \sqrt{\sum_{i=1}^{N-1} \left| \frac{1}{H} \int_0^H f_i dy - f_i^T \right|^2}$ ;
  | for  $i \leftarrow 1$  to  $N - 1$  do
  | | if  $\frac{1}{H} \int_0^H f_i dy < f_i^T$  then
  | | |  $f_{i0} = f_{i0} + \Delta f_0$ ;
  | | else
  | | |  $f_{i0} = f_{i0} - \Delta f_0$ ;
  | | end
  | end
end

```

tures having $f_L^T \leq 0.50$, the RMSD values for the linear model (dashed lines) are larger than that of the quadratic model (dotted lines). However, for compositions in the range $f_L^T \geq 0.50$, the linear model (dashed lines) exhibits lower RMSD values compared to the quadratic model (dotted lines) except for $\rho = 5.0$. In that case, the RMSD value of the linear model is smaller than the quadratic only for $f_L^T = 0.80$. The RMSD value decreases with increase in f_L^T (total composition of light species) for the linear empirical model for all four density ratios. The RMSD for the quadratic model, on the other hand, appears to increase with increasing f_L^T . This quantitative measurement confirms our qualitative observations discussed above, where we observe that the linear empirical model works well for mixtures with high composition of light particles, whereas the quadratic model works better for mixtures with low composition of light species. The particle force-based theory, however, shows that RMSD values remain nearly constant and do not vary with the composition of the mixture. The RMSD value using the particle force-based model is significantly smaller compared to the other two empirical approaches across the wide range of compositions and density ratios considered in this study. The above results for binary mixtures confirm that particle force-based theory is able to capture the segregation much more accurately compared to the empirical model for a wide range of composition and density ratios.

We next report results for ternary mixtures. Figure 11 shows the steady state concentration profiles for a ternary mixture having an equal composition of the three species. The data corresponds to a density ratio of $\rho_H : \rho_M : \rho_L = 3 : 2 : 1$ and inclination angle of $\theta = 25^\circ$. Figure 11a shows the concentration profile of light species, whereas figures 11b and 11c show that of the medium and the heavy species, respectively. Theoretical predictions using the linear empirical segregation model (dashed lines) differ from the DEM data (symbols) for light and medium species in the ternary mixture. Such differences are not observable for the heavy species. On the other hand, predictions using the particle force-based segregation model (solid lines) and quadratic empirical segregation model (dotted lines) match with the DEM results very well for all three species of the mixture. These observations can be confirmed by the RMSD values reported in the legends of figure 11. While the RMSD values for the heavy species are found to be nearly identical for all three segregation models, the linear empirical model RMSD values are found to be significantly higher than the other two models for both light as well as medium-density species. We also find that RMSD values for the quadratic empirical model are not very different from the RMSD values of the particle force-based theory for all three species. These results confirm that both the quadratic empirical model and the particle force-based model are capable of accurately predicting segregation

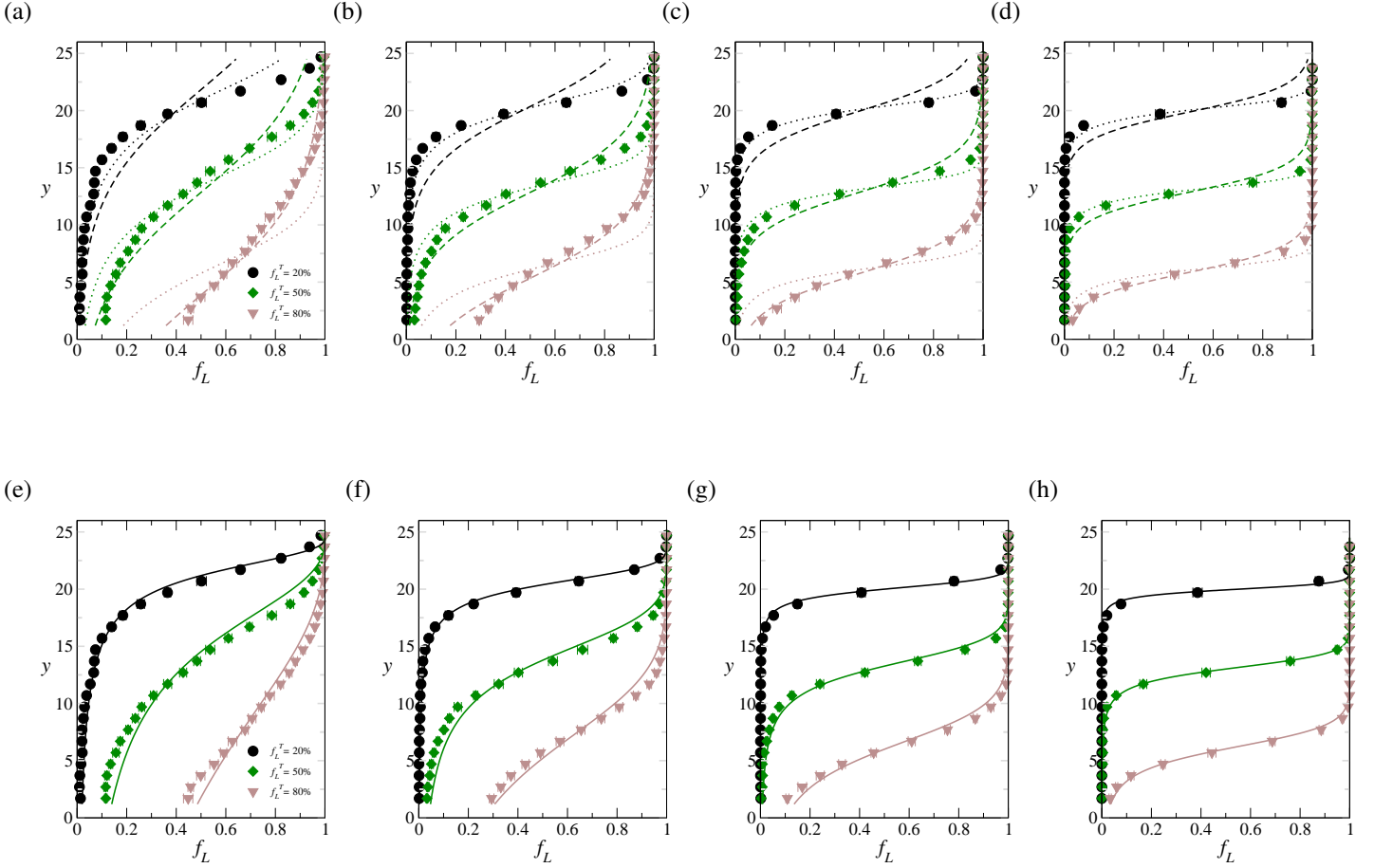


Figure 9: (a-d) Comparison of theoretical predictions using linear (dashed lines) and quadratic (dotted) empirical approach along with (e-h) theoretical predictions of particle force-based segregation model (solid lines) with DEM simulation data (symbols). The results are shown for the three different mixture compositions $f_L^T = 0.20$ (black), 0.50 (green) and 0.80 (brown) for binary mixtures having density ratio $\rho = 1.5$ in (a,e), $\rho = 2.0$ in (b,f), $\rho = 3.0$ in (c,g), and $\rho = 5.0$ in (d,h) at inclination angle $\theta = 25^\circ$.

for equal composition ternary mixture. In order to explore the applicability of the empirical model over a wide range of mixture compositions, we select mixtures with 70% composition of a particular species and 20% and 10% of the other two species. We obtain the theoretical predictions for each of these mixtures and compare them with their DEM simulations.

Figure 12a shows the results for the mixture with 70% of light species i.e., $f_L^T = 0.70$ with $f_M^T = 0.20$ & $f_H^T = 0.10$. Theoretical predictions using the linear empirical segregation model (dashed lines) match well with the DEM data for all three species. In contrast to the equal composition mixtures case, the quadratic empirical segregation model predictions (dotted lines) deviate strongly from the DEM results and particle force-based segregation model predictions. In this case, the quadratic approach fails to capture the DEM results throughout the entire layer height. Figure 12b shows predictions for the mixture with 70% medium species composition; the heavy and light species composition being 20% and 10%, respectively. For this mixture, the predictions using the quadratic empirical model as well as the linear empirical model differ substantially from the DEM data for both light (blue) and medium (red) species. On the other hand, the predictions based on the particle force

model exhibit very good match with the DEM data. Figure 12c shows the results for a ternary mixture where the composition of heavy species is 70% and that of the light species is 20%. Predictions using the quadratic approach for the light species are found to be in good agreement with DEM data. Differences for the medium-density and high-density species are noticeable. The linear empirical segregation model (dashed line) shows significant deviation for all three species. Theoretical predictions obtained using the particle force-based model exhibit excellent agreement with the DEM data for all three species for this case as well. These observations can be confirmed by comparing the RMSD values of the three models for each of the mixtures. Figure 13 shows the RMSD value for the light (blue), medium (red) and heavy (green) species for each segregation model. In all the cases, the RMSD value for the particle force-based theory is much smaller compared to both the empirical models. This confirms that the particle force-based segregation model is able to capture the segregation of various kinds of mixtures. In contrast, the linear and quadratic empirical models seem to work well in some cases and fail in some other situations.

In order to understand the inability of the quadratic model to predict concentration in the mixtures rich in either in light

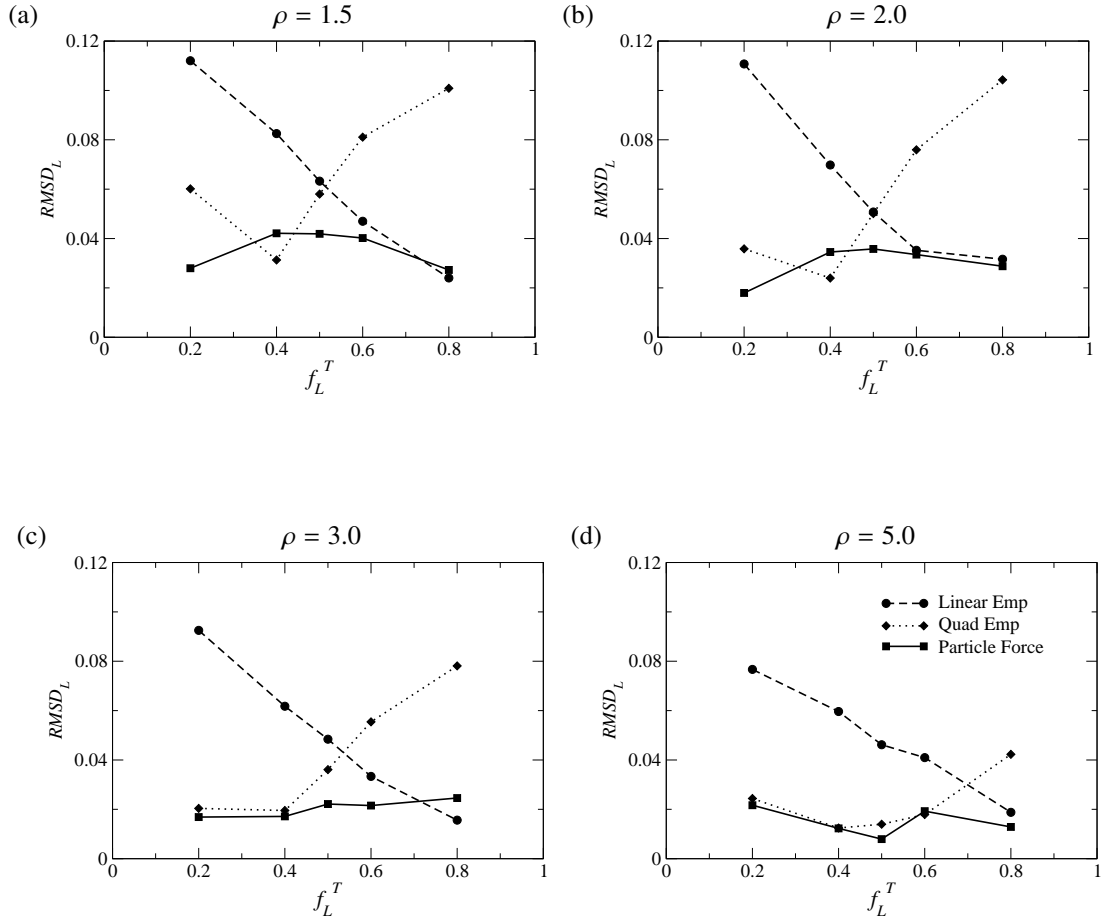


Figure 10: Variation of light species root mean square deviation (RMSD) value with mixture composition for three different segregation model density ratios (a) $\rho = 1.5$, (b) $\rho = 2.0$, (c) $\rho = 3.0$, and (d) $\rho = 5.0$. Solid lines correspond to the particle force-based model, whereas the dashed and the dotted lines correspond to the linear and quadratic empirical models, respectively.

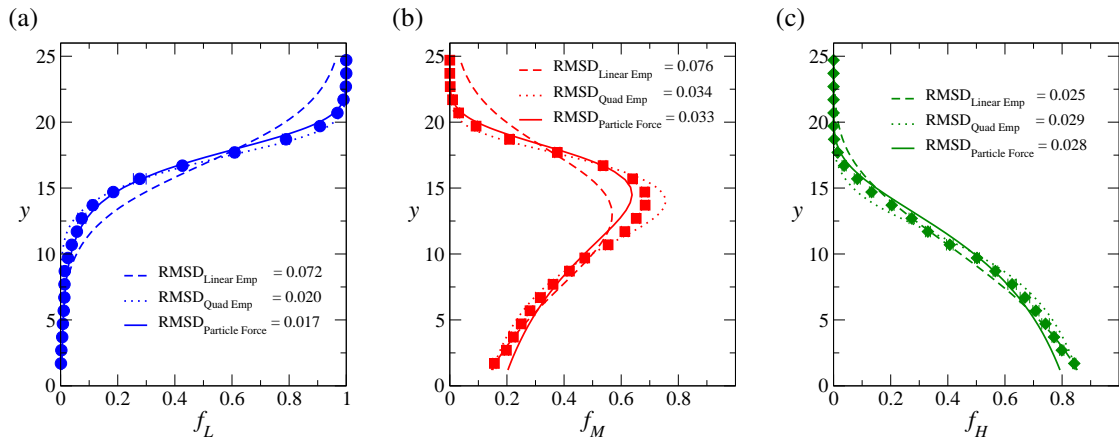


Figure 11: Comparison of theoretical predictions using linear (dashed lines) and quadratic (dotted) empirical model along with the particle force-based model (solid lines) with DEM simulation data (symbols) for equal composition ternary mixture of density ratio $\rho_H : \rho_M : \rho_L = 3 : 2 : 1$. Concentration profile of (a) light-density species, (b) medium-density species, and (c) high-density species for $\theta = 25^\circ$.

or in medium species, we plot the shear rate scaled segregation velocity of the heavy species for four different compositions of binary mixtures in figure 14a. Data have been shown for a

binary mixture of density ratio $\rho = 1.5$ flowing over an inclination angle of $\theta = 25^\circ$. Different symbols correspond to different mixture compositions. Evidently, the variation of the shear rate

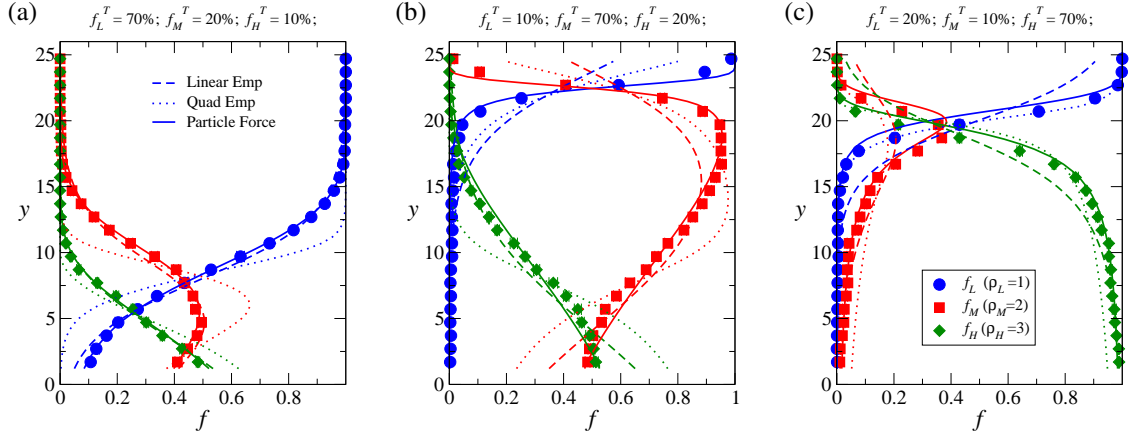


Figure 12: Comparison of theoretical predictions using linear (dashed lines) and quadratic (dotted lines) empirical model along with the particle force-based model (solid lines) with DEM simulation data (symbols) for three different compositions in a ternary mixture of density ratio $\rho_H : \rho_M : \rho_L = 3 : 2 : 1$. Blue circles correspond to light species while red squares and green diamonds correspond to medium and heavy species. Concentration profiles for (a) $f_L^T = 70\%$, $f_M^T = 20\%$, $f_H^T = 10\%$, (b) $f_L^T = 10\%$, $f_M^T = 70\%$, $f_H^T = 20\%$, and (c) $f_L^T = 20\%$, $f_M^T = 10\%$, $f_H^T = 70\%$.

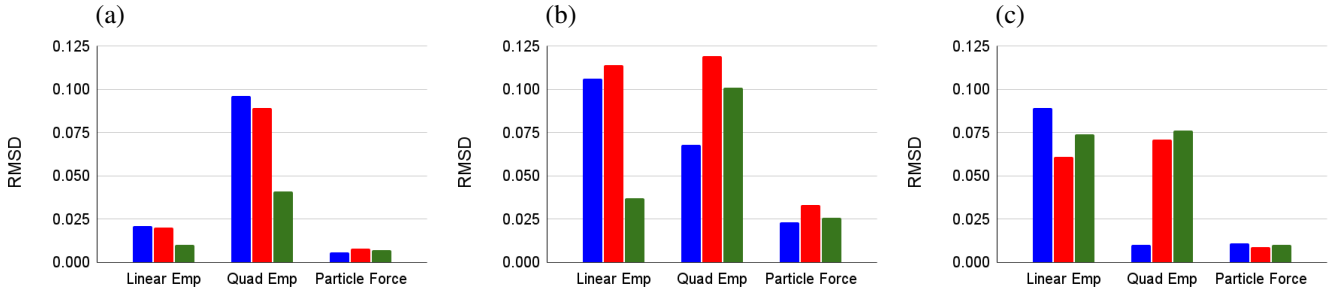


Figure 13: The root mean square deviation (RMSD) values for light (blue), medium (red) and heavy (green) species using three different segregation models in ternary mixtures of density ratio $\rho_H : \rho_M : \rho_L = 3 : 2 : 1$. Three different mixture compositions of (a) $f_L^T = 70\%$, $f_M^T = 20\%$, $f_H^T = 10\%$, (b) $f_L^T = 10\%$, $f_M^T = 70\%$, $f_H^T = 20\%$, and (c) $f_L^T = 20\%$, $f_M^T = 10\%$, $f_H^T = 70\%$ are considered.

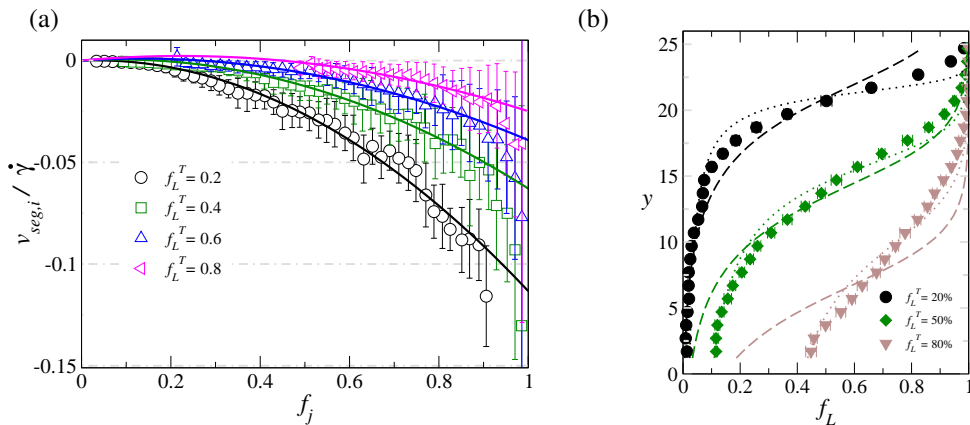


Figure 14: (a) Shear scaled segregation velocity of heavy species for different composition mixture. Symbols represent DEM data, and solid lines represent the quadratic empirical fits of form $v_{seg,i}/\dot{\gamma} = df_j(A_{ij} + B_{ij})f_j$. (b) Steady-state concentration profiles of light species in a binary mixture of density ratio $\rho = 1.5$. Symbols represent DEM data. Lines represent quadratic empirical model predictions. Dashed lines correspond to the empirical parameters estimated by averaging data over a wide range of compositions while dotted lines correspond to empirical parameters estimated for individual mixture compositions of light species.

scaled segregation velocity is different for different compositions of the mixture. For example, the value of $v_{seg,i}/\dot{\gamma}$ for a mixture composition of $f_L^T = 0.8$ is less than one-fourth of the value for a composition mixture of $f_L^T = 0.2$. The magnitude of $v_{seg,i}/\dot{\gamma}$ of heavy species decreases with an increase in the composition of light species in the mixture. Hence the empirical parameters obtained for different mixture compositions are expected to show significant differences.

f_L^T	0.20	0.40	0.50	0.60	0.80
A_{HL}	0.013	0.040	0.037	0.032	0.037
B_{HL}	-0.132	-0.123	-0.101	-0.084	-0.070

Table 4: Quadratic empirical parameters for heavy species for five different composition mixtures of density ratio $\rho = 1.5$.

Table 4 shows the parameters for each composition obtained by fitting the quadratic model to the data shown in figure 14a. Solid lines in figure 14a show the fitted quadratic curve using the values reported in Table 4. Figure 14b shows the predictions obtained using the quadratic empirical parameters for the respective composition of the mixture using dotted lines. The predictions match accurately with DEM data for all three compositions. However, employing the averaged empirical parameters across all the compositions, the predictions (shown by dashed lines) deviate significantly from the DEM data. The RMSD values for the dashed lines (using the same parameters for all compositions) are found to be 0.06, 0.06, & 0.10 for $f_L^T = 20\%$, 50% , and 80% mixtures, respectively. However, using the values corresponding to the mixture composition, the RMSD values reduce to 0.05, 0.04, & 0.03, respectively. Our analysis confirms that the large RMSD values for $f_L^T > 0.5$ in the quadratic empirical model case shown in figure 10 can be attributed to this concentration dependence of the parameters. For example, using the revised parameters for $\rho = 3.0$ and $f_L^T = 80\%$ mixture (figure 10c) reduces the RMSD value to 0.02 from 0.08. Thus we conclude that the quadratic empirical parameters indeed depend on the total composition of the species in the mixture. This is in contrast to the observations reported by Jones et al. (2018) who reported that the inlet composition in heap flow does not affect the empirical segregation velocity relation for quadratic segregation models. A similar comparison for the linear empirical model, however, does not show the dependency of the fitted parameters on mixture composition. This is in agreement with Xiao et al. (2016) who showed that the RMSD values for the predictions do not change significantly when using the linear empirical parameters obtained for individual composition.

5. Conclusion

In this study, we have investigated the suitability of empirical segregation models for predicting segregation in periodic chute flows. This simple system allows us to explore the effect of the inclination angle, different initial configurations, and the duration of measurement on the segregation parameters. We explore the two existing empirical approaches by accounting

for or ignoring diffusional contribution in the computation of segregation velocity $v_{seg,i}$ from DEM simulations. While the parameters are estimated using transient data in the case of the linear empirical model, the quadratic model uses steady-state data for estimating the parameters. We find that the time period of measurement of $v_{seg,i}$ affects the values of the empirical parameters estimated in the case of the linear empirical model. In addition, the initial configuration also seems to have a significant effect on the estimated values of these parameters. The appropriate values of empirical parameters in the case of the linear empirical model can be obtained by measuring percolation velocity for approximately twice the segregation time scale in a system starting with mixed configuration. The other configurations should be avoided for determining the linear empirical model parameters. The quadratic model parameters, however, are found to be less sensitive to the initial configurations used. In addition, the time scale of observation does not affect these values as well since steady-state data are used.

Using the appropriate values of empirical parameters for both the empirical models, we predict the concentration profiles for mixtures of different compositions and density ratios. In addition, we also predict the concentration profile from the particle force-based segregation model. We compute RMSD values to quantify the deviation of the predicted profiles with the corresponding DEM simulation data. A comparison of the RMSD values shows that the empirical model RMSD values are significantly larger than those of the particle force-based model predictions. The linear empirical model has a larger RMS deviation for mixtures rich in heavy species. The quadratic empirical model predictions have larger RMS deviation in the case of mixture rich in light species. The deviation in the quadratic model case arises due to the dependence of empirical parameters on mixture composition and can be substantially reduced by using parameters corresponding to the specific composition.

We also compare the predictions of the empirical segregation models and particle force-based theory with DEM simulations for ternary mixtures. While the linear empirical as well as particle force-based models have been used to predict segregation in multi-component mixtures, the quadratic model predictions have been restricted to binary mixtures only. We extended the methodology to predict segregation in the case of ternary mixtures using quadratic empirical model. A comparison of the predictions from these three segregation models for ternary mixtures of different compositions reconfirms that the particle force-based theory is able to predict the simulation data in much better agreement compared to the empirical models. Owing to the fact that the segregation model in the particle force-based approach is obtained from the forces acting on the particles, the species segregation velocity in this approach accounts for the effect of the inclination angle and viscosity dependence on local mixture composition. Such effects are not accounted in the empirical approach.

A similar comparison of empirical and particle force-based segregation models also needs to be done for mixtures having different sizes. It remains to be seen whether the dependencies of the segregation parameters on the measurement time, initial configuration, and inclination angle are observable for empiri-

cal models in the case of size segregation. In addition, mixtures differing in both size and density also need to be considered. While empirical models for such mixtures have been proposed, a particle force-based theory for the combined effect of size and density is still lacking and will be reported in the near future. Finally, the particle force-based theory also needs to be explored in few other flow configurations to establish its applicability in experimentally realizable systems.

Funding. AT gratefully acknowledges the financial support provided by the Indian Institute of Technology Kanpur via the initiation grant IITK/CHE/20130338. AT and SK gratefully acknowledge the funding support provided to SK by the Prime Minister’s Research Fellowship (Government of India) grant.

Declaration of Interest. The authors report no conflict of interest.

Author ORCIDs.

Soniya Kumawat <https://orcid.org/0000-0003-3314-9875>;

Vishnu Kumar Sahu <https://orcid.org/0000-0002-7768-0505>;

Anurag Tripathi <https://orcid.org/0000-0001-9945-3197>.

References

- Baxter, J., Tüzün, U., Heyes, D., Hayati, I., Fredlund, P., 1998. Stratification in poured granular heaps. *Nature* 391, 136–136.
- Bridgwater, J., Foo, W.S., Stephens, D.J., 1985. Particle mixing and segregation in failure zones—theory and experiment. *Powder technology* 41, 147–158.
- Chen, H., Zhao, X.q., Xiao, Y.g., Liu, Y.l., Liu, Y., 2016. Radial mixing and segregation of granular bed bi-dispersed both in particle size and density within horizontal rotating drum. *Transactions of Nonferrous Metals Society of China* 26, 527–535.
- Deng, Z., Fan, Y., Theuerkauf, J., Jacob, K.V., Umbanhowar, P.B., Lueptow, R.M., 2020. Modeling segregation of polydisperse granular materials in hopper discharge. *Powder Technology* 374, 389–398.
- Deng, Z., Umbanhowar, P.B., Ottino, J.M., Lueptow, R.M., 2018. Continuum modelling of segregating tridisperse granular chute flow. *Proceedings of the Royal Society A: Mathematical, Physical and Engineering Sciences* 474, 20170384.
- Deng, Z., Umbanhowar, P.B., Ottino, J.M., Lueptow, R.M., 2019. Modeling segregation of polydisperse granular materials in developing and transient free-surface flows. *AIChE Journal* 65, 882–893.
- Duan, Y., Jing, L., Umbanhowar, P.B., Ottino, J.M., Lueptow, R.M., 2022. Segregation forces in dense granular flows: closing the gap between single intruders and mixtures. *Journal of Fluid Mechanics* 935.
- Duan, Y., Umbanhowar, P.B., Ottino, J.M., Lueptow, R.M., 2020. Segregation models for density-bidisperse granular flows. *Physical Review Fluids* 5, 044301.
- Duan, Y., Umbanhowar, P.B., Ottino, J.M., Lueptow, R.M., 2021. Modelling segregation of bidisperse granular mixtures varying simultaneously in size and density for free surface flows. *Journal of Fluid Mechanics* 918, A20.
- Fan, Y., Hill, K.M., 2015. Shear-induced segregation of particles by material density. *Phys. Rev. E* 92, 022211.
- Fan, Y., Jacob, K.V., Freireich, B., Lueptow, R.M., 2017. Segregation of granular materials in bounded heap flow: A review. *Powder Technology* 312, 67–88.
- Fan, Y., Schlick, C.P., Umbanhowar, P.B., Ottino, J.M., Lueptow, R.M., 2014. Modelling size segregation of granular materials: the roles of segregation, advection and diffusion. *J. Fluid Mech.* 741, 252–279.
- Fry, A.M., Umbanhowar, P.B., Ottino, J.M., Lueptow, R.M., 2018. Effect of pressure on segregation in granular shear flows. *Physical Review E* 97, 062906.
- Fry, A.M., Umbanhowar, P.B., Ottino, J.M., Lueptow, R.M., 2019. Diffusion, mixing, and segregation in confined granular flows. *AIChE Journal* 65, 875–881.
- Gajjar, P., Gray, J.M.N.T., 2014. Asymmetric flux models for particle-size segregation in granular avalanches. *J. Fluid Mech.* 757, 297–329.
- Gao, S., Ottino, J.M., Umbanhowar, P.B., Lueptow, R.M., 2021. Modeling granular segregation for overlapping species distributions. *Chemical Engineering Science* 231, 116259.
- Gray, J.M.N.T., Ancy, C., 2011. Multi-component particle-size segregation in shallow granular avalanches. *Journal of Fluid Mechanics* 678, 535–588.
- Gray, J.M.N.T., Chugunov, V.A., 2006. Particle-size segregation and diffusive remixing in shallow granular avalanches. *Journal of Fluid Mechanics* 569, 365–398.
- Jain, A., Metzger, M.J., Glasser, B.J., 2013. Effect of particle size distribution on segregation in vibrated systems. *Powder technology* 237, 543–553.
- Jones, R.P., Isner, A.B., Xiao, H., Ottino, J.M., Umbanhowar, P.B., Lueptow, R.M., 2018. Asymmetric concentration dependence of segregation fluxes in granular flows. *Phys. Rev. Fluids* 3, 094304.
- Pereira, G., Tran, N., Cleary, P., 2014. Segregation of combined size and density varying binary granular mixtures in a slowly rotating tumbler. *Granular Matter* 16, 711–732.
- Sahu, V.K., Kumawat, S., Agrawal, S., Tripathi, A., 2023. Particle force-based density segregation theory for multi-component granular mixtures in a periodic chute flow. *Journal of Fluid Mechanics* 956, A8.
- Savage, S., Lun, C., 1988. Particle size segregation in inclined chute flow of dry cohesionless granular solids. *Journal of fluid mechanics* 189, 311–335.
- Schlick, C.P., Fan, Y., Isner, A.B., Umbanhowar, P.B., Ottino, J.M., Lueptow, R.M., 2015a. Modeling segregation of bidisperse granular materials using physical control parameters in the quasi-2d bounded heap. *AIChE Journal* 61, 1524–1534.
- Schlick, C.P., Fan, Y., Umbanhowar, P.B., Ottino, J.M., Lueptow, R.M., 2015b. Granular segregation in circular tumblers: theoretical model and scaling laws. *J. Fluid Mech* 765, 632–652.
- Schlick, C.P., Isner, A.B., Freireich, B.J., Fan, Y., Umbanhowar, P.B., Ottino, J.M., Lueptow, R.M., 2016. A continuum approach for predicting segregation in flowing polydisperse granular materials. *Journal of Fluid Mechanics* 797, 95–109.
- Staron, L., Phillips, J.C., 2014. Segregation time-scale in bi-disperse granular flows. *Physics of Fluids* 26, 033302.
- Tai, C., Hsiau, S., Kruelle, C., 2010. Density segregation in a vertically vibrated granular bed. *Powder Technology* 204, 255–262.
- Tripathi, A., Khakhar, D.V., 2011a. Numerical simulation of the sedimentation of a sphere in a sheared granular fluid: a granular stokes experiment. *Phys. Rev. Lett.* 107, 108001.
- Tripathi, A., Khakhar, D.V., 2011b. Rheology of binary granular mixtures in the dense flow regime. *Physics of Fluids* 23, 113302.
- Tripathi, A., Khakhar, D.V., 2013. Density difference-driven segregation in a dense granular flow. *J. Fluid Mech.* 717, 643–669.
- Tripathi, A., Kumar, A., Nema, M., Khakhar, D.V., 2021. Theory for size segregation in flowing granular mixtures based on computation of forces on a single large particle. *Phys. Rev. E* 103, L031301.
- Utter, B., Behringer, R.P., 2004. Self-diffusion in dense granular shear flows. *Physical Review E* 69, 031308.
- Van der Vaart, K., Gajjar, P., Epely-Chauvin, G., Andreini, N., Gray, J.M.N.T., Ancy, C., 2015. Underlying asymmetry within particle size segregation. *Phys. Rev. Lett.* 114, 238001.
- Wiederseiner, S., Andreini, N., Epely Chauvin, G., Moser, G., Monnereau, M., Gray, J.M.N.T., Ancy, C., 2011. Experimental investigation into segregating granular flows down chutes. *Physics of Fluids* 23, 013301.
- Xiao, H., Fan, Y., Jacob, K.V., Umbanhowar, P.B., Kodam, M., Koch, J.F., Lueptow, R.M., 2019. Continuum modeling of granular segregation during hopper discharge. *Chemical Engineering Science* 193, 188–204.
- Xiao, H., Umbanhowar, P.B., Ottino, J.M., Lueptow, R.M., 2016. Modelling density segregation in flowing bidisperse granular materials. *Proceedings of the Royal Society A: Mathematical, Physical and Engineering Sciences* 472, 20150856.
- Yang., S., 2006. Density effect on mixing and segregation processes in a vibrated binary granular mixture. *Powder Technology* 164, 65–74.

Appendix A. Effect of diffusivity values on segregation predictions

Fan et al. (2014) and Gao et al. (2021) considered both spatially varying diffusivity values as well as a constant diffusivity value in the prediction of binary size segregation using linear empirical model. The authors report that the spatial variation in the diffusivity has a negligible effect on the predictions of the continuum model in the case of quasi-2D heap flows. Table S1 shows that while the mean diffusivity values for a given inclination do not differ a lot from each other due to change in mixture composition, the effect of inclination on the mean diffusivity is very significant and hence needs to be accounted for if one wishes to use a constant diffusivity.

f_L^T	0.20	0.40	0.50	0.60	0.80
$\theta = 25^\circ$	0.0121	0.0114	0.0113	0.0114	0.0127
$\theta = 29^\circ$	0.0361	0.0325	0.0321	0.0322	0.0345

Table S1: Mean diffusivity (D_{avg}) values for five different binary mixture compositions at two different inclination angles $\theta = 25^\circ$ and 29° .

Figure S1 shows the comparison of theoretical predictions using particle force-based theory using both constant as well as spatially varying diffusivity across the layer. Data are shown for three different binary mixtures having light species composition $f_L^T = 0.20$ (black), $f_L^T = 0.50$ (green), and $f_L^T = 0.80$ (brown) with density ratio $\rho = 3.0$. Figure S1a shows the predictions at inclination angle $\theta = 25^\circ$ while figure S1b shows the predictions at inclination angle $\theta = 29^\circ$. Solid lines represent the theoretical predictions accounting for the spatial variation of the diffusivity using the relation $D = b\dot{\gamma}d_{mix}^2$. The dashed lines represent the predictions using a constant value of average diffusivity D_{avg} corresponding to the inclination angle for 50% – 50% binary mixture. Both solid and dashed lines accurately match with the DEM data (symbols) for all three composition mixtures at two different inclination angles.

Dotted lines in figure S1a correspond to predictions obtained using D_{avg} for $\theta = 29^\circ$ instead of 25° . The discrepancy from the DEM simulation data (symbols) is evident. This mismatch confirms that using the average value of diffusivity at one angle for predicting segregation of mixtures flowing at another angle gives highly inaccurate results. Similarly, using data for D_{avg} corresponding to $\theta = 25^\circ$ to predict segregation for $\theta = 29^\circ$ case also leads to highly inaccurate predictions (figure S1b). The difference is attributed to the fact that the diffusivity values at $\theta = 29^\circ$ are nearly three times larger than $\theta = 25^\circ$ case. This indicates that accounting for the variation of the diffusivity with the shear rate using the relation $D = b\dot{\gamma}d_{mix}^2$ should be preferred as it captures the influence of the inclination angle on the diffusivity as well.

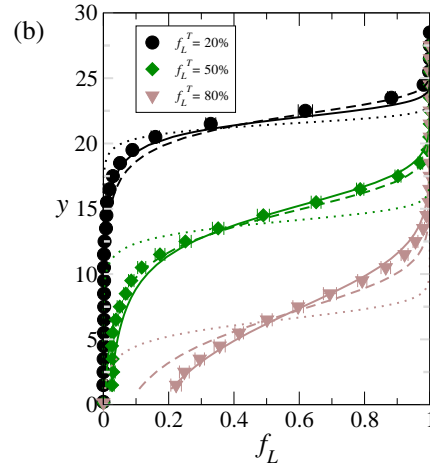
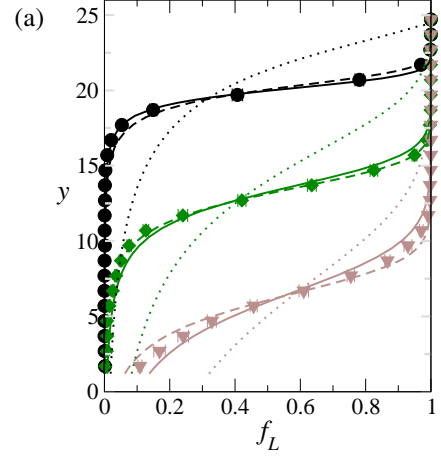


Figure S1: Comparison of theoretical predictions using a constant diffusivity and a spatially varying diffusivity $D = b\dot{\gamma}d_{mix}^2$ for a binary mixture of density ratio $\rho = 3.0$ for (a) $\theta = 25^\circ$ and (b) $\theta = 29^\circ$. Symbols represent DEM data, solid lines represent the predictions using spatially varying diffusivity $D = b\dot{\gamma}d_{mix}^2$. Dashed lines represent the predictions using constant diffusivity D corresponding to inclination angle θ for 50% – 50% binary mixture. Dotted lines represent the predictions using a constant value of diffusivity D taken for $\theta = 29^\circ$ in (a) and $\theta = 25^\circ$ in (b).